ERJ Express. Published on January 11, 2019 as doi: 10.1183/13993003.00786-2018

EUROPEAN RESPIRATORY *journal*

FLAGSHIP SCIENTIFIC JOURNAL OF ERS

Early View

Original article

Neutrophils Disturb Pulmonary Microcirculation in Sepsis-induced Acute Lung Injury

Inwon Park, Mingyo Kim, Kibaek Choe, Eunjoo Song, Howon Seo, Yoonha Hwang, Jinhyo Ahn, Seung-Hyo Lee, Jae Hyuk Lee, You Hwan Jo, Kyuseok Kim, Gou Young Koh, Pilhan Kim

Please cite this article as: Park I, Kim M, Choe K, *et al*. Neutrophils Disturb Pulmonary Microcirculation in Sepsis-induced Acute Lung Injury. *Eur Respir J* 2019; in press (https://doi.org/10.1183/13993003.00786-2018).

Neutrophils Disturb Pulmonary Microcirculation in Sepsis-induced Acute Lung Injury

Authors: Inwon Park[1], Mingyo Kim[4], Kibaek Choe[2,3], Eunjoo Song[2,3], Howon Seo[2,3], Yoonha Hwang[2,3], Jinhyo Ahn[2,3], Seung-Hyo Lee[1], Jae Hyuk Lee[5], You Hwan Jo[5], Kyuseok Kim[5], Gou Young Koh[1,6,*], and Pilhan Kim[1,2,3,*]

Affiliations:

[1]Graduate School of Medical Science and Engineering, Korea Advanced Institute of Science and Technology (KAIST), Daejeon, 34141, Republic of Korea

[2]Graduate School of Nanoscience and Technology, Korea Advanced Institute of Science and Technology (KAIST), Daejeon, 34141, Republic of Korea

[3]KI for Health Science and Technology (KIHST), Korea Advanced Institute of Science and Technology (KAIST), Daejeon, 34141, Republic of Korea

[4]Division of Rheumatology, Department of Internal Medicine, Gyeongsang National University School of Medicine, Jinju, Gyeongsangnam-do, 52727, Republic of Korea

[5]Department of Emergency Medicine, Seoul National University Bundang Hospital (SNUBH), Seongnam-si, Gyeonggi-do, 13620, Republic of Korea

[6]Center for Vascular Research, Institute for Basic Science (IBS), Daejeon, 34141, Republic of Korea

*To whom correspondence should be addressed:
Pilhan Kim, Graduate School of Nanoscience and Technology, KAIST, 291 Daehak-ro, Daejeon, 34141, Republic of Korea, Phone: 82-42-350-1115; Email: pilhan.kim@kaist.ac.kr.

Gou Young Koh, Center for Vascular Research, IBS; Graduate School of Medical Science and Engineering, KAIST, 291 Daehak-ro, Daejeon, 34141, Republic of Korea, Phone: 82-42-350-2638, E-mail:gykoh@kaist.ac.kr

Summary: Neutrophils induce dead space in the pulmonary microcirculation in sepsis-induced ALI, recovered by a Mac-1 inhibitor.

Abstract:

The lung is highly vulnerable during sepsis, yet its functional deterioration accompanied by disturbances in the pulmonary microcirculation are poorly understood. This study aimed to investigate how the pulmonary microcirculation is distorted in sepsis-induced acute lung injury (ALI) and reveal the underlying cellular pathophysiologic mechanism.

Using a customized intravital lung microscopic imaging system in a murine model of sepsis-induced ALI, we achieved direct real-time visualization of the pulmonary microcirculation and circulating cells *in vivo*. We derived the functional capillary ratio (FCR) as a quantitative parameter for assessing the fraction of functional microvasculature in the pulmonary microcirculation and dead space.

We identified that the FCR rapidly decreases in the early stage of sepsis-induced ALI. The intravital imaging revealed that it was the result of the generation of dead space which was induced by prolonged neutrophil entrapment within the capillaries. We further showed that the neutrophils had an extended sequestration time and an arrest-like dynamic behavior, both of which triggered neutrophil aggregates inside the capillaries and arterioles. Finally, we found that Mac-1 (CD11b/CD18) was upregulated in the sequestered neutrophils and that a Mac-1 inhibitor restored the FCR and improved the hypoxemia.

With the intravital lung imaging system, we observed how Mac-1 upregulated neutrophil aggregates led to the generation of dead space in the pulmonary microcirculation and its improvement by a Mac-1 inhibitor in sepsis-induced ALI.

Introduction

Sepsis is one of the most unaffordable conditions of hospitalization and the foremost contributor to hospital death, representing a major worldwide health burden [1, 2]. Sepsis is a syndrome characterized by a dysregulated response of the host to invading pathogens which involves hemodynamic alterations that lead to multiple life-threatening organ dysfunctions [3, 4]. Among the injured organs, the lung is the first and most frequent organ to fail. Accompanying acute respiratory distress syndrome (ARDS), which is the clinical term for acute lung injury (ALI), is one of the most critical prognostic factors for mortality in patients with sepsis [5]. Despite intense research efforts aimed at treating sepsis-induced ARDS, a lung supportive ventilation strategy remains a mainstay of treatment, and no effective therapies aimed at the microcirculation to directly improve the ventilation-perfusion mismatch are available in ARDS [6]. Although it has been identified that 'dead space' assessment could provide significant clinical value in ARDS [6, 7], until now, it has remained a hypothesis in terms of an impairment of the lung alveoli that are ventilated but not perfused. Admittedly, ARDS is a poorly understood syndrome with regard to the association between lung injury and microcirculation [6, 8]. Recently, a study reported evidence of thrombi in the pulmonary vasculature which was limited as an *ex vivo* study, and to date, the *in vivo* process of neutrophil influx and the consequent disturbance in the pulmonary microcirculation remain to be investigated [9, 10].

Unregulated recruitment and activation of neutrophils could induce organ injury through the release of inflammatory mediators, including cytokines and reactive oxygen species (ROS) [11, 12]. Yet, our knowledge on the detailed dynamic behavior of neutrophils in the pulmonary microcirculation is mostly limited to speculation gleaned from observations in the systemic circulation [13]. Because the diameter of neutrophils is greater than that of the pulmonary capillaries, neutrophils must deform to pass through the capillaries, which is a

relatively time-consuming process [14]. This process, referred to as neutrophil sequestration, was originally described for cells other than the freely circulating group of neutrophils within the lung and has been observed, to some extent, using macroscopic radiolabeling imaging devices [15]. Indeed, previous studies have demonstrated neutrophil sequestration in lung capillaries; however, their mechanism of how a neutrophil sequestration event leads to ARDS remains limited [16, 17]. Therefore, considering the importance and obscurity of the pulmonary microcirculation in ARDS, understanding the changes in the pulmonary microcirculation including the dynamic behavior of neutrophils is imperative for elucidating the pathophysiology, which may lead to novel treatment strategies for sepsis-induced ARDS [18].

To investigate the pulmonary microcirculation in sepsis-induced ARDS, we used a custom-designed video-rate laser scanning confocal microscope in combination with a micro-suction-based pulmonary imaging window [19, 20]. Using the intravital lung imaging system, we directly identified the alteration of the microcirculatory perfusion in a murine sepsis-induced ALI model and demonstrated the role of Mac-1 upregulated neutrophils in the pulmonary microcirculation, which suggests the clinical potential of a Mac-1 inhibitor as a therapeutic drug for sepsis-induced ALI.

Materials and Methods

Mice

All animal experiments were performed in accordance with the standard guidelines for the care and use of laboratory animals and were approved by the Institutional Animal Care and Use Committee (IACUC) of KAIST (protocol No. KA2014-30 and KA2016-55). All mice were individually housed in ventilated and temperature & humidity-controlled cages (22.5 °C, 52.5 %) under 12:12h light:dark cycle and provided with standard diet and water *ad libitum*. For experimental use, 8–20 weeks old male mice (20~30 g) were utilized in this study. C57BL/6N mice were purchased from OrientBio (Suwon, Rep. of Korea) and Tie2-GFP mice (Stock No. 003658, Jackson Laboratory) where the GFP is expressed under endothelium-specific Tie2 promotor were purchased from the Jackson Laboratory. $LysM^{GFP/+}$ mouse was generously provided by Prof. M. Kim (University of Rochester, U.S.A.).

Animal models

To generate sepsis-induced ALI model [12], high-dose LPS (10 mg/kg, *E. coli* serotype 055:B5, L2880, Sigma-Aldrich) or high-grade CLP model was utilized. Details are provided in the online data supplement.

Fluorescent dye and antibody utilized in intravital imaging

In vivo labeling of erythrocytes, vasculature, neutrophils (Ly6G), CD11b, CD18, DHE, and modeling of neutrophil depletion and Mac-1 inhibition treatment is described in the online data supplement.

Flow Cytometry, Histological Analysis, and Arterial Blood Gas Analysis

Details are provided in the online data supplement.

Imaging System and Intravital Pulmonary Imaging

To visualize *in vivo* pulmonary microcirculation through pulmonary imaging window, a custom-built video-rate laser-scanning confocal microscopy system was implemented [21, 22]. Additional details of imaging system and preparation of mouse for intravital pulmonary imaging are provided in the online data supplement.

Image Processing

Functional capillary imaging analysis was performed using real-time movie of DiD-labeled erythrocytes flowing in capillaries. After splitting colors of movie, sequential images of channels detecting DiD was processed by a median filter with a radius of two pixels to enhance the signal-to-noise ratio. Maximal intensity projection of 600 to 900 (20 – 30 seconds) frames was generated to show the functional capillary perfused by erythrocytes. Functional capillary ratio (FCR) was determined by calculating the ratio of functional capillary area (DiD-labeled RBC) to the total capillary area (vessel area detected by Tie2 or Dextran signaling). All image processing to calculate FCR was performed by ImageJ (https://imagej.nih.gov/ij/). Image rendering with three-dimensional reconstruction, track analysis of erythrocytes and neutrophils, and plotting track displacement was conducted with IMARIS 8.2 (Bitplane). Additional details of image processing are provided in the online data supplement.

Statistical Analysis

All data are presented as mean ± SD or median ± interquartile range, as appropriate to represent values of the group respectively. Statistical differences between means or medians were determined by unpaired 2-tailed Student's t-test, Mann-Whitney test, one-way ANOVA with post hoc Holm-Sidak's multiple comparisons, or Kruskal-Wallis test with post hoc

Dunn's multiple comparison tests, as appropriate. Statistical significance was set at $P < 0.05$, and analysis was performed with Prism 6.0 (GraphPad).

Results

The functional capillary ratio is decreased in the pulmonary microcirculation in sepsis-induced ALI

The cellular dynamics in the pulmonary microcirculation were investigated *in vivo* in mice using a custom-built intravital video-rate laser scanning confocal microscopy system [19, 20]. Erythrocytes were sampled from a Tie2-GFP transgenic donor mouse by cardiac puncture. After labeling with DiD, adoptive transfer was performed into a syngenic recipient mouse by the tail vein [23] (figure 1a). Rapidly flowing DiD-labeled erythrocytes were clearly visible inside the pulmonary vessel in which the endothelial cells were labeled with GFP in real-time, enabling the acquisition of spatiotemporal information on the flowing trajectory and velocity of individual erythrocytes (figure 1b). The track information was acquired *in vivo* for multiple erythrocytes simultaneously and analyzed (figure 1c and supplemental video 1).

Next, we used a murine endotoxin-induced indirect lung injury model to investigate the changes in the erythrocyte flow in the pulmonary microcirculation in sepsis [12]. Six hours after the administration of 10 mg/kg of intraperitoneal LPS, intravital pulmonary imaging was performed using DiD-labeled erythrocytes that were injected during the imaging. Though no significant difference was found in the mean velocity of the erythrocytes between the control and LPS groups (figure 1d), the erythrocyte perfusion pattern dramatically changed in the LPS-treated mice (supplemental Video 2). To determine and quantify the perfusion area, erythrocytes in sequential images from 600 frames (20 seconds) were presented in a maximal intensity projection manner (supplemental figure 1a and b). The control group exhibited

widespread and diffuse characteristics of perfusion, whereas the distribution of perfusion in the LPS-treated mice was more concentrated and overlapped with arterioles and a few capillaries (figure 1e). Next, we defined a parameter termed the functional capillary ratio (FCR) as a quantitative measure of the pulmonary microcirculation, which was calculated from the ratio of the functional capillary area, as determined by the erythrocyte trajectory (DiD, red), to the total capillary area (Tie2, green). A decreased FCR, which represents abnormal perfusion, was observed in the sepsis-induced ALI group even though there was not a large difference in the total capillary area (figure 1f and g). Furthermore, we confirmed that our FCR results correspond to hypoxemia and hypercapnia from the arterial blood gas analysis in the left ventricle [12] (figure 1h and i).

Entrapped neutrophils in pulmonary capillaries induce microcirculatory disturbances in sepsis-induced ALI

During the imaging to measure the FCR in the sepsis-induced ALI mice, we observed several sites of capillary obstruction in the magnified view. These obstructions were induced by objects inside the capillaries that could represent the primary pathophysiological mechanism underlying the decreased FCR in the early stage of ALI development. Because neutrophils rapidly respond to systemic inflammation, we postulated that the objects that induced the obstruction could be neutrophils [13]. Real-time intravital imaging of the pulmonary capillaries in a naive $LysM^{GFP/+}$ animal showed transient entrapment of neutrophils in the capillary during circulation [24, 25] (figure 2a and supplemental video 3). During the period in which the capillaries became obstructed, circulating cells, which were assumed to be predominantly erythrocytes, could not flow through the capillaries. However, capillary flow resumed after the neutrophils passed through the capillaries. In contrast, in the sepsis-induced ALI model of mice in which neutrophil recruitment was augmented, the flow of the cells in

the pulmonary microcirculation was interrupted in numerous spots (figure 2b and c, and supplemental video 4). Thus, during early inflammation, when innate immune cells are recruited, we identified neutrophils as the primary obstacle in the microcirculation in pulmonary capillaries.

Intravascular neutrophil motility initially increases and later decreases to arrest during the early development of sepsis-induced ALI

To investigate the dynamic behaviors of individual neutrophils during entrapment in the pulmonary capillary, we performed a total of 30 minutes of time-lapse imaging of neutrophils in the pulmonary microcirculation 3 and 6 hours after LPS administration (figure 3a and b, and supplemental video 5). Given that the flow velocity of the erythrocytes was high (>500 μm/s), we determined that neutrophils that were detected continuously for more than 2 minutes were not flowing; rather, they were sequestered (i.e., crawling or marginating inside the vessel). Time-lapse imaging showed that the proportion of sequestered neutrophils, as well as their individual sequestration times in the LPS group, dramatically increased compared to the PBS control group, in which most of the neutrophils were sequestered briefly (figure 3c and d). Interestingly, during sequestration, the motility of the 3 h LPS neutrophils increased, as determined by the track displacement length (figure 3b and e), track length (figure 3f), and mean velocity (figure 3g). However, as sepsis progressed, the 6 h LPS neutrophils became less motile, and the track length and velocity decreased. In addition, the meandering index decreased in a timely manner, which was influenced by an increased sequestration time and the arrest characteristics of the neutrophils (figure 3h). Taken together, these data show that, during the early period of endotoxin-induced ALI, neutrophils begin to activate and become motile inside the capillaries; however, in the late period, they gradually begin to arrest inside the capillaries.

Neutrophils obstruct pulmonary vessels, generate circulatory dead space, and release ROS in situ in sepsis-induced ALI

Using the intravital imaging of the pulmonary microcirculation 3 to 6 hours after LPS administration, we observed for the first time the entire process of dead space formation in the pulmonary microcirculation. In the capillaries, a circulating neutrophil became trapped on one side of a vessel in which the other side was already obstructed by another neutrophil, revealed by real-time imaging (figure 4a and supplemental video 6). The flow stopped between the two neutrophils, thereby generating a circulatory dead space. At some capillary sites, we observed clusters of neutrophils where no flow was detected (supplemental figure 2a). Such obstructions were not limited to the capillaries, but was also observed in the branching regions of the arterioles that were connected to the capillaries (supplemental figure 2b and c). Over the course of 10 minutes of time-lapse intravital imaging, we observed that neutrophils quickly blocked the branching sites and disturbed the microcirculation near the obstructed region (figure 4b and supplemental video 7). To confirm the correlation of neutrophil sequestration and dead space formation, we injected DiD-labeled erythrocytes and visualized the functional capillary (figure 4c and supplemental video 8). Functional capillary mapping and track path analysis demonstrated that neutrophil-induced capillary and arteriole obstruction generated circulatory dead space.

Next, to identify the function and activation of the entrapped neutrophils, we investigated ROS production in the sequestered neutrophils. Using our intravital imaging system, we detected ROS generation in intravascular neutrophils in the lungs *in situ* [26] (figure 4d). Compared to the control group, in which ROS was undetectable in transiently sequestered neutrophils, both the number and proportion of ROS-generating neutrophils were dramatically increased in the LPS-treated mice (figure 4e and f). In contrast to the previous

understanding of ROS production by neutrophils at the site of inflammation [27], our findings suggest that ROS production had been initiated in much earlier stage because of the development of neutrophil entrapment in the capillary. The findings also imply that entrapped neutrophils could release ROS *in situ*, which could harm the endothelial cells and adjacent intravascular structure before extravasation.

Neutrophil depletion improves the pulmonary microcirculation in sepsis-induced ALI

To further confirm the essential role of neutrophils in capillary blockade, we investigated the pulmonary microcirculation in a neutrophil-depleted (N-Dep) mouse model. Injecting 200 μg of a Ly6G-specific monoclonal antibody (1A8) 24 hours before imaging led to neutrophil depletion [28] (supplemental figure 3). Using antibodies, neutrophils were depleted in the $LysM^{GFP/+}$ mice 24 hours before LPS injection, and then intravital imaging was performed 6 hours after LPS injection (figure 5a). Consistent with our hypothesis, neutrophil depletion improved the FCR in the LPS treatment group; this was repeatedly verified by magnified imaging (figure 5b and c, and supplemental video 9). The number of LysM+ cells decreased to a certain level after neutrophil depletion, but there was not complete depletion because of remnant LysM+ cells (figure 5d), which were presumably alveolar macrophages in the extravascular spaces [24, 25] (figure 5b, magnified). Nevertheless, our results indicate that the decreased number of LysM+ cells, mostly intravascular neutrophils, leads to an improved FCRs in the pulmonary microcirculation (figure 5d). These data support that neutrophils function as the main components of aggregates and the primary blockers of flow in the pulmonary microcirculation during systemic inflammation.

Mac-1-upregulated neutrophils are sequestered in the lung in sepsis-induced ALI

Although neutrophil depletion increased the FCR, bench-to-bedside clinical translation of the neutrophil depletion strategy is not feasible [13]. Therefore, to identify the target for subsets of sequestered neutrophils, we isolated two groups of neutrophils in a single mouse (figure 6a). We hypothesized that the integrin expression pattern of neutrophils in the left ventricle that had already passed through the pulmonary capillary may be different from the pattern of neutrophils in the lung, where sequestration occurs. Flow cytometry was performed for the two groups of neutrophils gated on Ly6G+ to investigate their integrin expression (figure 6b and supplemental figure 4). We found that the baseline expression of CD11b and CD18 was upregulated in the neutrophils in the LPS group. Interestingly, in the same mouse, the neutrophils in the lung expressed higher levels of CD11b and CD18 compared to the neutrophils in the left ventricle (figure 6d and e). Intravital pulmonary imaging (Figure 6g and h) confirmed that the neutrophils sequestered in the lung in the LPS mice expressed high levels of CD11b and CD18, in agreement with our flow cytometry findings (Figure 6i–l). Thus, compared to circulating neutrophils, neutrophils sequestered in the lung had an upregulated expression of Mac-1 (CD11b/CD18) integrins in the sepsis-induced ALI model.

Mac-1 inhibitor restores the FCR in the pulmonary microcirculation in sepsis-induced ALI

Given that Mac-1 is upregulated in neutrophils that are sequestered in the lung, we investigated the effects of a Mac-1 inhibitor on the pulmonary microcirculation. To extend our findings to a polymicrobial sepsis model, we performed intravital lung imaging on a cecal ligation and puncture (CLP) mouse model. As in the LPS model, the FCR was significantly lower in the CLP mouse model than in the control (figure 7a and b). Administration of an anti-CD11b antibody (5 mg/kg, IP) [29] and abciximab (10 mg/kg, IP) [30-32], a cross-reactive inhibitor for the binding of various ligands to Mac-1, restored the FCR with less

sequestration of Ly6G+ cells (figure 7c). To further confirm our findings, the FCR was calculated at the same site and found to be significantly increased after the injection of abciximab (10 mg/kg, IV) (figure 7d and e, and supplemental video 10). Arterial blood gas analysis in the left ventricle confirmed that the FCR results were in accordance with hypoxemia and hypercapnia, suggesting that abciximab increases gas exchange in this sepsis-induced ALI mouse model through an improvement in the microcirculation (figure 7f and g). Furthermore, pulmonary edema after 24 hours of injury was significantly ameliorated in the Mac-1 inhibitor model in accordance with previous results (supplemental figure 5).

Discussion

Despite differences between the systemic and pulmonary capillary network, most of our knowledge of the microcirculation in sepsis has come from studies of the systemic circulation, with decreased functional capillary density (FCD) and increased intercapillary areas [33]. Although our study of the pulmonary microcirculation during sepsis partially agrees with findings from the systemic circulation, the underlying etiology of the microcirculatory change is distinct from that of the systemic circulation. Previously, endothelial dysfunction and vasoconstriction were suggested as potential central mechanisms in impaired systemic microcirculation [34]. Our results suggest that cluster formation of recruited neutrophils also has a key detrimental role in the pulmonary microcirculation in the early stage of sepsis-induced ALI.

Even though previous studies suggested that sequestration in pulmonary capillaries functions as a defensive immune surveillance system for detecting pathogens in the circulation, it could not explain how neutrophil sequestration progresses to ARDS [14, 35]. In contrast, our study shows that neutrophils form clusters and act as an obstacle in capillaries and arterioles,

leading to the redistribution and obstruction of the pulmonary microcirculation, highlighting the novel detrimental role of neutrophils. Recently, studies have revealed the cluster of neutrophils inside the pulmonary vasculature from the lung biopsies of patients with ARDS [10] and murine fungal sepsis [36] which supports our results regarding the aggregate formation of neutrophils. The neutrophil-induced obstruction of flow increases the mismatching areas of ventilation and perfusion, thereby intensifying hypoxia due to sepsis-induced ARDS. Compared to previous intravital imaging studies on the adhesion of neutrophils in the pulmonary capillary [37, 38], our study clearly shows how dead space with ventilation/perfusion mismatch is created in the microcirculation by neutrophils. Moreover, we can directly image the dead space fraction, which has been estimated indirectly by the difference in the partial pressure of arterial versus exhaled carbon dioxide using volumetric capnography.

Although our results imply that neutrophil depletion improves the pulmonary circulation, there is considerable debate about the effects of treatment-induced neutrophil depletion in sepsis because the effects on bacterial clearance and the response to systemic inflammation are unclear [39]. Accordingly, we evaluated the subpopulation of neutrophils that may ameliorate lung injury [40]. Flow cytometry showed that Mac-1 (CD11b/CD18), which interacts with ICAM-1 in endothelial cells and various coagulation factors, was significantly upregulated in the sequestered neutrophils in lungs from the ALI model and could be the potential target integrin for improving the pulmonary microcirculation. Previous studies have investigated the role of L-selectin and CD11/CD18 in neutrophil sequestration and revealed that neither was required for the initial immediate sequestration occurring within 1 minute in the pulmonary capillaries. However, once the neutrophils were sequestered, L-selectin and CD11/CD18 were critical for the adherence of neutrophils within the capillary bed for more

than 4 to 7 minutes [14, 41]. Additionally, several studies have suggested the inhibition of Mac-1 as a treatment for protecting against neutrophil infiltration in lung injury during sepsis [42, 43]. In contrast to indirect assays utilized in previous studies, our research used real-time intravital microscopic imaging to show that the inhibition of Mac-1 reduced neutrophil sequestration, increased the FCR and offered protection from ALI. However, a recent study reported on neutrophil-platelet interactions in thrombosis in the pulmonary vasculature [10, 44], raising concerns about whether platelets in thrombosis may have a confounding effect and whether the effects of abciximab, also known as GP IIb/IIIa inhibitor, are the consequence of thrombus resolution due to interactions with platelets. There may be platelets that were not identified in our study; nevertheless, most of the flow disturbances we observed were resolved by neutrophil depletion. This implies that neutrophils have an essential role in augmenting cluster formation inside pulmonary capillaries in sepsis-induced ALI [36]. Moreover, because we found that anti-CD11b and abciximab elicited equivalent improvements in the FCR, it seems that the effects of abciximab could be attributed to its anti-Mac-1 activity on neutrophils. Nevertheless, due to unavailability of platelet imaging, we were not able to identify the involvement of platelets in the formation of neutrophil cluster bridging between neutrophils, and thereby the additional effect of abciximab targeting not only the neutrophil through CD11b but also the platelets through GP IIb/IIIa cannot be ruled out. Additional intravital lung imaging should be performed to further elucidate neutrophil-platelet thrombogenesis *in vivo* to gain a better understanding of the relevant pathophysiology and subsequent molecular targets in the pulmonary vasculature. Furthermore, abciximab has the advantageous position that it is already FDA approved for use during coronary intervention to prevent thrombosis, which brings our study much closer to the clinical field.

In conclusion, the use of a custom-designed real-time intravital lung microscopic imaging system enabled direct visualization of prolonged neutrophil entrapment in capillaries during sepsis-induced ALI in mice. The resulting disturbance in flow in the pulmonary microcirculation correlated with dead space. Furthermore, this finding provides novel insights into how capillary entrapment of neutrophils contributes to pulmonary microcirculatory disturbances. This system could serve as a useful tool for investigating diseases that affect the pulmonary microcirculation and could be used to evaluate potential treatments for sepsis-induced ARDS.

Supplemental Materials

Supplemental Figure 1. Mapping of functional capillary ratio (FCR) according to number of frames.

Supplemental Figure 2. Identification of neutrophil aggregates in capillary and arteriole.

Supplemental Figure 3. Confirmation of neutrophil depletion in $LysM^{GFP/+}$ model.

Supplemental Figure 4. Flow cytometry gating strategy to isolate neutrophil.

Supplemental Figure 5. Assessment of pulmonary edema in Mac-1 inhibition.

Supplemental Video 1. Real-time intravital imaging of DiD-labeled erythrocytes in pulmonary microcirculation

Supplemental Video 2. Reduction of functional capillary ratio in pulmonary microcirculation in sepsis-induced ALI model.

Supplemental Video 3. Neutrophil entrapment in capillary disturbs flow.

Supplemental Video 4. Increased neutrophil entrapment induces capillary obstruction in sepsis-induced ALI model.

Supplemental Video 5. Alteration of neutrophil dynamics in sepsis-induced ALI model.

Supplemental Video 6. Neutrophils block capillary and trigger dead space formation in sepsis-induced ALI model.

Supplemental Video 7. Neutrophils induce cluster formation *in situ* in the arteriole in sepsis-induced ALI model.

Supplemental Video 8. Capillary and arteriole obstruction of neutrophil aggregates induces dead space formation in sepsis-induced ALI model.

Supplemental Video 9. Depletion of neutrophil increases FCR of pulmonary microcirculation.

Supplemental Video 10. Abciximab improves pulmonary microcirculation in sepsis-induced ALI model.

Acknowledgements

The authors thank Seonghye Kim (SNUBH) for her technical assistance during revisional experiment. The authors also thank Soyeon Ahn, Jieun Moon, Eunji Kong, Jingu Lee, Ryul Kim, Sujung Hong (KAIST) for advice and helpful discussion, Soo Yun Lee and Haeun Kim (KAIST) for their technical assistance.

Author contributions

I.P. performed the experiments, analyzed data, and wrote the manuscript. M.K. and S-H.L. performed and analyzed the flow cytometry experiments. K.C., E.S., H.S., Y.H., and J.A. performed the experiments and implemented the customized confocal microscopy. J.H.L., Y.H.J., and K.K. reviewed the manuscript and adviced the study. G.Y.K. and P.K. conceived the study, designed the experiments, interpreted data, and reviewed the manuscript. All authors provided substantial contributions to either: 1) the conception or design of the work, or the acquisition, analysis or interpretation of data for the work; 2) revised the manuscript critically for important intellectual content; 3) approved the final version of manuscript; and 4) agreed to be accountable for all aspects of the work

Conflict of interest

All authors declare that they have no competing financial interests that might have influenced the performance or presentation of the work described in this manuscript.

Support statement

This research was supported by the Health Fellowship Foundation and the Global Ph.D. Fellowship Program (NRF-2015H1A2A1030717) through the National Research Foundation of Korea (NRF) funded by the Ministry of Education, Republic of Korea and the Global Frontier Project (NRF-2013M3A6A4044716), Basic Research Program (NRF-2017R1E1A1A01074190) funded by the Ministry of Science and ICT, Republic of Korea, and Korea Healthcare Technology R&D Project (HI15C0399) funded by Ministry of Health and Welfare, Republic of Korea.

References

1. Torio CM, Moore BJ. National Inpatient Hospital Costs: The Most Expensive Conditions by Payer, 2013: Statistical Brief #204. Healthcare Cost and Utilization Project (HCUP) Statistical Briefs, Rockville (MD), 2016.
2. Hall MJ, Levant S, DeFrances CJ. Trends in inpatient hospital deaths: National Hospital Discharge Survey, 2000-2010. *NCHS Data Brief* 2013(118): 1-8.
3. Singer M, Deutschman CS, Seymour CW, Shankar-Hari M, Annane D, Bauer M, Bellomo R, Bernard GR, Chiche JD, Coopersmith CM, Hotchkiss RS, Levy MM, Marshall JC, Martin GS, Opal SM, Rubenfeld GD, van der Poll T, Vincent JL, Angus DC. The Third International Consensus Definitions for Sepsis and Septic Shock (Sepsis-3). *JAMA* 2016: 315(8): 801-810.
4. Angus DC, van der Poll T. Severe sepsis and septic shock. *N Engl J Med* 2013: 369(9): 840-851.
5. Lagu T, Rothberg MB, Shieh MS, Pekow PS, Steingrub JS, Lindenauer PK. Hospitalizations, costs, and outcomes of severe sepsis in the United States 2003 to 2007. *Crit Care Med* 2012: 40(3): 754-761.
6. Thompson BT, Chambers RC, Liu KD. Acute Respiratory Distress Syndrome. *N Engl J Med* 2017: 377(6): 562-572.
7. Nuckton TJ, Alonso JA, Kallet RH, Daniel BM, Pittet JF, Eisner MD, Matthay MA. Pulmonary dead-space fraction as a risk factor for death in the acute respiratory distress syndrome. *N Engl J Med* 2002: 346(17): 1281-1286.
8. Ryan D, Frohlich S, McLoughlin P. Pulmonary vascular dysfunction in ARDS. *Ann Intensive Care* 2014: 4: 28.
9. Matthay MA, Ware LB, Zimmerman GA. The acute respiratory distress syndrome. *J Clin Invest* 2012: 122(8): 2731-2740.
10. Yuan Y, Alwis I, Wu MCL, Kaplan Z, Ashworth K, Bark D, Jr., Pham A, McFadyen J, Schoenwaelder SM, Josefsson EC, Kile BT, Jackson SP. Neutrophil macroaggregates promote widespread pulmonary thrombosis after gut ischemia. *Sci Transl Med* 2017: 9(409).
11. Grommes J, Soehnlein O. Contribution of neutrophils to acute lung injury. *Mol Med* 2011: 17(3-4): 293-307.
12. Matute-Bello G, Downey G, Moore BB, Groshong SD, Matthay MA, Slutsky AS, Kuebler WM, Acute Lung Injury in Animals Study G. An official American Thoracic Society workshop report: features and measurements of experimental acute lung injury in animals. *Am J Respir Cell Mol Biol* 2011: 44(5): 725-738.
13. Phillipson M, Kubes P. The neutrophil in vascular inflammation. *Nat Med* 2011: 17(11): 1381-1390.
14. Doerschuk CM. Mechanisms of leukocyte sequestration in inflamed lungs. *Microcirculation* 2001: 8(2): 71-88.
15. MacNee W, Selby C. New perspectives on basic mechanisms in lung disease. 2. Neutrophil traffic in the lungs: role of haemodynamics, cell adhesion, and deformability. *Thorax* 1993: 48(1): 79-88.
16. Kuebler WM, Borges J, Sckell A, Kuhnle GE, Bergh K, Messmer K, Goetz AE. Role of L-selectin in leukocyte sequestration in lung capillaries in a rabbit model of endotoxemia. *Am J Respir Crit Care Med* 2000: 161(1): 36-43.
17. Lien DC, Henson PM, Capen RL, Henson JE, Hanson WL, Wagner WW, Jr., Worthen GS. Neutrophil kinetics in the pulmonary microcirculation during acute inflammation. *Lab Invest* 1991: 65(2): 145-159.
18. Looney MR, Bhattacharya J. Live imaging of the lung. *Annu Rev Physiol* 2014: 76: 431-445.

19. Kim P, Puoris'haag M, Cote D, Lin CP, Yun SH. In vivo confocal and multiphoton microendoscopy. *J Biomed Opt* 2008: 13(1): 010501.
20. Han S, Lee SJ, Kim KE, Lee HS, Oh N, Park I, Ko E, Oh SJ, Lee YS, Kim D, Lee S, Lee DH, Lee KH, Chae SY, Lee JH, Kim SJ, Kim HC, Kim S, Kim SH, Kim C, Nakaoka Y, He Y, Augustin HG, Hu J, Song PH, Kim YI, Kim P, Kim I, Koh GY. Amelioration of sepsis by TIE2 activation-induced vascular protection. *Sci Transl Med* 2016: 8(335): 335ra355.
21. Veilleux I, Spencer JA, Biss DP, Cote D, Lin CP. In Vivo Cell Tracking With Video Rate Multimodality Laser Scanning Microscopy. *IEEE Journal of Selected Topics in Quantum Electronics* 2008: 14(1): 10-18.
22. Park I, Choe K, Seo H, Hwang Y, Song E, Ahn J, Hwan Jo Y, Kim P. Intravital imaging of a pulmonary endothelial surface layer in a murine sepsis model. *Biomed Opt Express* 2018: 9(5): 2383-2393.
23. Seo H, Hwang Y, Choe K, Kim P. In vivo quantitation of injected circulating tumor cells from great saphenous vein based on video-rate confocal microscopy. *Biomed Opt Express* 2015: 6(6): 2158-2167.
24. Faust N, Varas F, Kelly LM, Heck S, Graf T. Insertion of enhanced green fluorescent protein into the lysozyme gene creates mice with green fluorescent granulocytes and macrophages. *Blood* 2000: 96(2): 719-726.
25. Kreisel D, Nava RG, Li W, Zinselmeyer BH, Wang B, Lai J, Pless R, Gelman AE, Krupnick AS, Miller MJ. In vivo two-photon imaging reveals monocyte-dependent neutrophil extravasation during pulmonary inflammation. *Proc Natl Acad Sci U S A* 2010: 107(42): 18073-18078.
26. Finsterbusch M, Hall P, Li A, Devi S, Westhorpe CL, Kitching AR, Hickey MJ. Patrolling monocytes promote intravascular neutrophil activation and glomerular injury in the acutely inflamed glomerulus. *Proc Natl Acad Sci U S A* 2016: 113(35): E5172-5181.
27. Mittal M, Siddiqui MR, Tran K, Reddy SP, Malik AB. Reactive oxygen species in inflammation and tissue injury. *Antioxid Redox Signal* 2014: 20(7): 1126-1167.
28. Daley JM, Thomay AA, Connolly MD, Reichner JS, Albina JE. Use of Ly6G-specific monoclonal antibody to deplete neutrophils in mice. *J Leukoc Biol* 2008: 83(1): 64-70.
29. Ahn GO, Tseng D, Liao CH, Dorie MJ, Czechowicz A, Brown JM. Inhibition of Mac-1 (CD11b/CD18) enhances tumor response to radiation by reducing myeloid cell recruitment. *Proc Natl Acad Sci U S A* 2010: 107(18): 8363-8368.
30. Peter K, Schwarz M, Conradt C, Nordt T, Moser M, Kubler W, Bode C. Heparin inhibits ligand binding to the leukocyte integrin Mac-1 (CD11b/CD18). *Circulation* 1999: 100(14): 1533-1539.
31. Schwarz M, Nordt T, Bode C, Peter K. The GP IIb/IIIa inhibitor abciximab (c7E3) inhibits the binding of various ligands to the leukocyte integrin Mac-1 (CD11b/CD18, alphaMbeta2). *Thromb Res* 2002: 107(3-4): 121-128.
32. Mickelson JK, Ali MN, Kleiman NS, Lakkis NM, Chow TW, Hughes BJ, Smith CW. Chimeric 7E3 Fab (ReoPro) decreases detectable CD11b on neutrophils from patients undergoing coronary angioplasty. *J Am Coll Cardiol* 1999: 33(1): 97-106.
33. De Backer D, Creteur J, Preiser JC, Dubois MJ, Vincent JL. Microvascular blood flow is altered in patients with sepsis. *Am J Respir Crit Care Med* 2002: 166(1): 98-104.
34. De Backer D, Orbegozo Cortes D, Donadello K, Vincent JL. Pathophysiology of microcirculatory dysfunction and the pathogenesis of septic shock. *Virulence* 2014: 5(1): 73-79.
35. Yipp BG, Kim JH, Lima R, Zbytnuik LD, Petri B, Swanlund N, Ho M, Szeto VG, Tak T, Koenderman L, Pickkers P, Tool ATJ, Kuijpers TW, van den Berg TK, Looney MR, Krummel MF, Kubes P. The Lung is a Host Defense Niche for Immediate Neutrophil-Mediated Vascular Protection. *Sci Immunol* 2017: 2(10).

36. Lee EKS, Gillrie MR, Li L, Arnason JW, Kim JH, Babes L, Lou Y, Sanati-Nezhad A, Kyei SK, Kelly MM, Mody CH, Ho M, Yipp BG. Leukotriene B4-Mediated Neutrophil Recruitment Causes Pulmonary Capillaritis during Lethal Fungal Sepsis. *Cell Host Microbe* 2018: 23(1): 121-133 e124.
37. Yang N, Liu YY, Pan CS, Sun K, Wei XH, Mao XW, Lin F, Li XJ, Fan JY, Han JY. Pretreatment with andrographolide pills((R)) attenuates lipopolysaccharide-induced pulmonary microcirculatory disturbance and acute lung injury in rats. *Microcirculation* 2014: 21(8): 703-716.
38. Gill SE, Rohan M, Mehta S. Role of pulmonary microvascular endothelial cell apoptosis in murine sepsis-induced lung injury in vivo. *Respir Res* 2015: 16: 109.
39. Robertson CM, Perrone EE, McConnell KW, Dunne WM, Boody B, Brahmbhatt T, Diacovo MJ, Van Rooijen N, Hogue LA, Cannon CL, Buchman TG, Hotchkiss RS, Coopersmith CM. Neutrophil depletion causes a fatal defect in murine pulmonary Staphylococcus aureus clearance. *J Surg Res* 2008: 150(2): 278-285.
40. Lewis SM, Khan N, Beale R, Treacher DF, Brown KA. Depletion of blood neutrophils from patients with sepsis: treatment for the future? *Int Immunopharmacol* 2013: 17(4): 1226-1232.
41. Kubo H, Doyle NA, Graham L, Bhagwan SD, Quinlan WM, Doerschuk CM. L- and P-selectin and CD11/CD18 in intracapillary neutrophil sequestration in rabbit lungs. *Am J Respir Crit Care Med* 1999: 159(1): 267-274.
42. Gao XP, Liu Q, Broman M, Predescu D, Frey RS, Malik AB. Inactivation of CD11b in a mouse transgenic model protects against sepsis-induced lung PMN infiltration and vascular injury. *Physiol Genomics* 2005: 21(2): 230-242.
43. Asaduzzaman M, Zhang S, Lavasani S, Wang Y, Thorlacius H. LFA-1 and MAC-1 mediate pulmonary recruitment of neutrophils and tissue damage in abdominal sepsis. *Shock* 2008: 30(3): 254-259.
44. Bennewitz MF, Jimenez MA, Vats R, Tutuncuoglu E, Jonassaint J, Kato GJ, Gladwin MT, Sundd P. Lung vaso-occlusion in sickle cell disease mediated by arteriolar neutrophil-platelet microemboli. *JCI Insight* 2017: 2(1): e89761.

Figure captions

Figure 1. Impaired pulmonary microcirculation in sepsis-induced ALI revealed by the functional capillary ratio (FCR). a) Schematics of intravital lung imaging experiment for pulmonary microcirculation visualization with adoptive transfer of DiD-labeled erythrocyte. **b**) Sequential images of rapidly flowing DiD-labeled erythrocyte (red) inside the pulmonary vessel (green) in Tie2-GFP mouse obtained in video-rate (30 frames/second). Scale bars, 100 μm. Time elapsed is indicated. **c**) Velocity color-coded track analysis of DiD-labeled erythrocyte in pulmonary microcirculation. Color represents the mean velocity of each segment of erythrocyte tracks (see also Supplemental Video 1). Scale bar, 100 μm. **d**) Comparison of mean velocity of RBC between PBS and LPS (10 mg/kg) group in the pulmonary microcirculation (n = 30, 10 field of view (FOV) per mouse, 3 mice per each group, P = 0.8157, two-tailed t-test). **e**) Representative functional capillary imaging in PBS and LPS group (see also Supplemental Video 2). The functional capillary was revealed by maximal intensity projection of real-time DiD-labeled erythrocyte imaging (see also Supplemental Figure 1a,b). White asterisks indicate dead spaces where the trajectory of erythrocyte was not observed. Scale bars, 100 μm. **f, g**) Comparisons of the ratio of the total capillary area and the functional capillary area between PBS and LPS group (n = 30, 10 FOV per mouse, 3 mice per each group, *P < 0.05, two-tailed t-test). **h, i**) Comparisons of the partial pressure of arterial O_2 and CO_2 at 6 hours after LPS between PBS (n = 6) and LPS group (n = 16) (*P < 0.05, Mann-Whitney test). All data are means ± s.d..

Figure 2. Entrapment of neutrophil inside the pulmonary capillary. a) Real-time imaging of $LysM^{GFP/+}$ (green) neutrophil entrapment in the pulmonary capillary (TMR dextran, red) (see also Supplemental Video 3). Each circulation inside capillary resumes after neutrophil in the upper region (^, blue) and the lower region (*****, red) has squeezed through the pulmonary

capillary. Scale bars, 10 μm. Dashed arrows indicate the direction of flow. Time elapsed is indicated in seconds. **b**) Representative intravital imaging of Ly6G+ cells (red) and consequent flow in pulmonary microcirculation (FITC Dextran, green) in PBS and LPS (10 mg/kg) group (see also Supplemental Video 4). Magnified spots consist of averaged imaging up to 30 frames and single frame imaging. Dashed arrows indicate the direction of flow. White arrowheads indicate entrapped neutrophils, and yellow arrowheads indicate obstructed capillary with no flow. Scale bars, 100 μm (Wide field) and 20 μm (Magnified spot). **c**) Comparison of number of Ly6G+ cells in pulmonary microcirculation between PBS and LPS group (n = 30, 10 FOV per mouse, 3 mice per each group, * P <0.05, two-tailed t-test). Data are means ± s.d..

Figure 3. Increased entrapment time and dynamically altered motility of neutrophil during the development of sepsis-induced ALI. a) Representative time-lapse imaging of Ly6G+ cells (red spots) in pulmonary microcirculation (FITC Dextran, green) in PBS, LPS 3 hours (LPS 3h), LPS 6 hours (LPS 6h) group (see also Supplemental Video 5). The color-coded track describes the motion of tracked Ly6G+ cells over a period of 30 minutes. Scale bars, 100 μm. **b**) Overlay of the track of Ly6G+ cells from a). Each track of Ly6G+ cells in a) is plotted from the central point and shows XY displacement. Scale bars, 10 μm. **c**) Histogram of track duration of Ly6G+ cell shown in a). **d-h**) Comparisons of sequestration time, track displacement length, track length, track velocity, and meandering index of Ly6G+ cells in pulmonary microcirculation in PBS, LPS 3h, and LPS 6h group (n = 466, 794, and 1076, respectively, 3 mice per each group, * P < 0.05, Kruskal-Wallis test with post hoc Dunn's multiple comparison test). Data are medians ± interquartile range.

Figure 4. Neutrophil aggregate in capillary and arteriole generates dead space and release ROS *in situ*. a) Representative real-time imaging of capillary obstruction with

Ly6G+ cells in sepsis-induced ALI model (see also Supplemental Video 6). Dashed arrow indicates the direction of flow. Yellow arrowheads indicate previously entrapped neutrophil and white arrowheads indicate newly appeared neutrophil obstructing capillary followed by dead space formation inside capillary. Dashed line indicates capillary of dead space. Scale bars, 20 μm. **b**) Representative time-lapse imaging of cluster formation by Ly6G+ cells in the branching region of arteriole connected to capillary (see also Supplemental Video 7). Dashed arrows indicate the direction of flow. Time elapsed is indicated as MM:SS (minute:second). Scale bars, 20 μm. **c**) Representative imaging of dead space generation triggered by cluster formation (see also Supplemental Video 8). White dashed circles indicate circulatory dead spaces. Dashed arrow indicates the direction of flow. Scale bars, 100 μm. **d**) Representative intravital imaging of ROS (blue, DHE) colocalized with neutrophil (red, Ly6G) in pulmonary microcirculation (green, FITC Dextran) in PBS and LPS group. Scale bars, 50 μm. **e** and **f**) Comparisons of number of ROS+ Ly6G+ cells and the ratio of ROS+ Ly6G+ cells to total Ly6G+ cells between PBS and LPS group (n = 30, 10 FOV per mouse, 3 mice per each group, * $P < 0.05$, two-tailed t-test). Data are means ± s.d..

Figure 5. Neutrophil depletion improves FCR of pulmonary microcirculation in sepsis-induced ALI model. a) Schematics of intravital lung imaging of neutrophil depletion in sepsis-induced ALI model. **b**) Representative intravital imaging of FCR in pulmonary microcirculation in PBS, LPS, N-dep, and N-dep + LPS group. Anatomical capillary (TMR Dextran, green), functional capillary (DiD-labeled erythrocyte, red), and LysM+ ($LysM^{GFP/+}$, magenta) cell imaging was acquired. White asterisks indicate dead spaces. Magnified images show entrapped LysM+ cells (arrowhead) and consequent flow disturbance (see also Supplemental Video 9). Scale bars, 20 μm in Magnified, and otherwise, 100 μm. **c**, **d**) Comparisons of FCR (%) and count of LysM+ cells among PBS, LPS, N-dep, and N-dep +

LPS group (n = 30, 10 FOV per mouse, 3 mice per each group, * P < 0.05, one-way ANOVA with post hoc Holm-Sidak's multiple comparisons test). Data are means ± s.d..

Figure 6. Mac-1 integrin is upregulated in entrapped neutrophil in pulmonary microcirculation. a) A schematic diagram showing isolation sampling of two groups of neutrophil (lung, blue; left ventricle:LV, red). **b**) Surface expression of integrin of Ly6G+ cells from lung and left ventricle. **c-f**) Comparisons of expression of integrin from flow cytometry in PBS and LPS group (n = 5 per each group, * P < 0.05, Mann-Whitney test). MFI, mean fluorescence intensity. Data are means ± s.d.. **g**, **h**) Representative three-dimensional intravital imaging of integrin in sequestered neutrophil. Cellular surface expression of CD11b (green) and CD18 (green) in Ly6G+ cells (red) is visualized *in vivo*. Scale bars, 100 μm. **i-l**) Comparisons of number of CD11b+Ly6G+ cells, CD18+Ly6G+ cells, and ratio of CD11b+Ly6G+ cell over total Ly6G+ cell and CD18+Ly6G+ cell over total Ly6G+ cell in PBS and LPS group (n = 9, 3 FOV per mouse, 3 mice per each group, * P < 0.05, Mann-Whitney test). Data are means ± s.d..

Figure 7. **Mac-1 inhibitor ameliorates FCR of pulmonary microcirculation in sepsis-induced ALI. a**) Representative intravital imaging of FCR in pulmonary microcirculation in Sham, Fc, Anti-CD11b, and Abciximab (Abc) group. Anatomical capillary (TMR Dextran, green), functional capillary (DiD-labeled erythrocyte, red), and neutrophil (Ly6G, magenta) imaging was acquired. White asterisks indicate dead spaces. Scale bars, 100 μm. **b**, **c**) Comparisons of FCR and number of Ly6G+ cells in pulmonary microcirculation. (n = 14-25, 3 mice per each group, * P < 0.05, two-tailed t-test). Data are means ± s.d.. **d**) Representative intravital lung imaging of Pre-Abc and Post-Abc group (see also Supplemental Video 10). White arrowheads indicate restoration of erythrocyte perfusion. Scale bars, 100 μm. **e**)

Comparison of FCR in Pre-Abc and Post-Abc group (n = 20 and 24, 6~8 FOV per mouse, 3 mice per each group respectively, * $P < 0.05$, two-tailed t-test). Data are means ± s.d.. **f**, **g**) Comparisons of the partial pressure of O_2 and CO_2 in Sham (n = 8), Fc (n = 10), and Abc (n = 6) group (* $P < 0.05$, Kruskal-Wallis test with post hoc Dunn's multiple comparison tests). Data are means ± s.d..

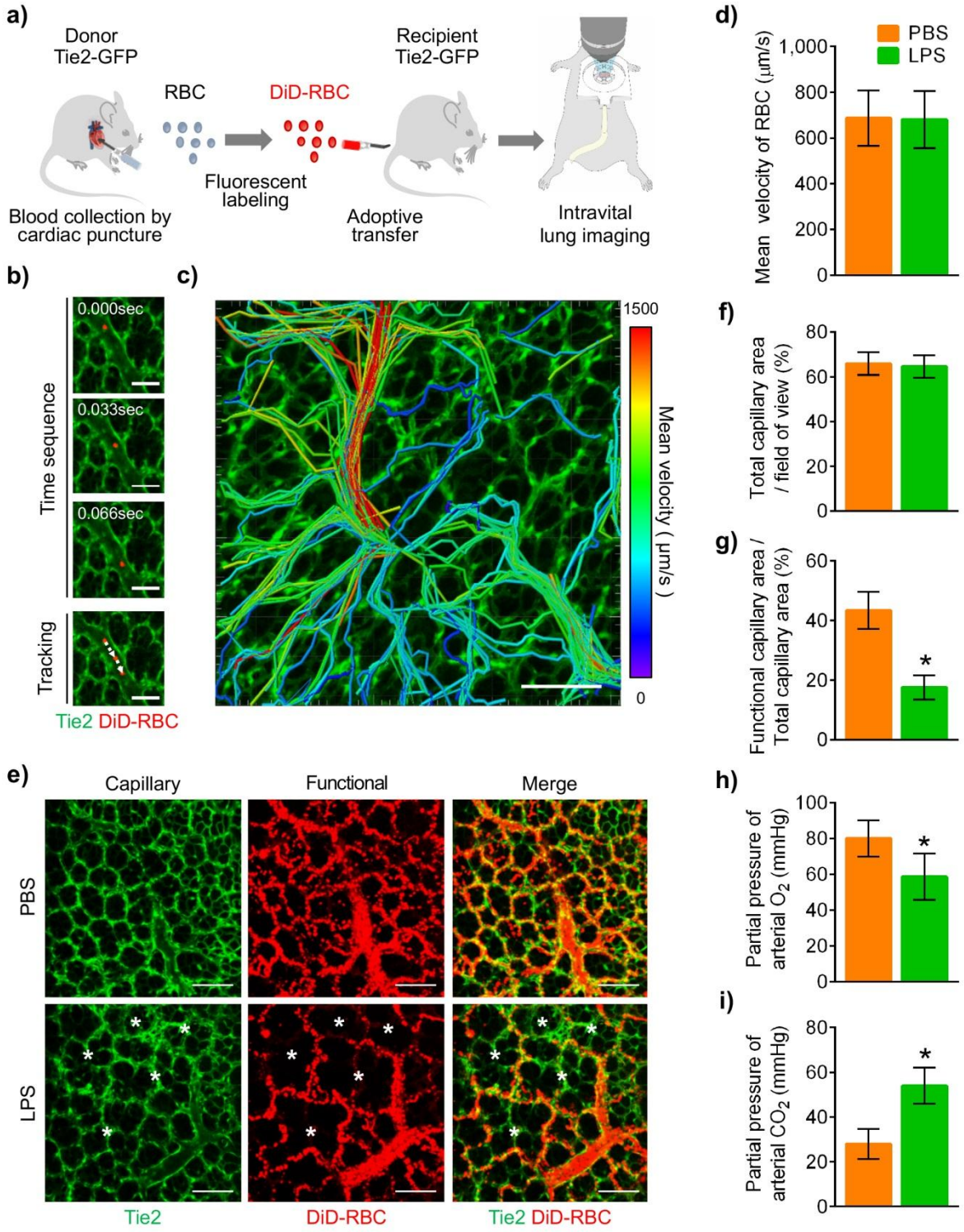
a)
Donor
Tie2-GFP
RBC
DiD-RBC
Recipient
Tie2-GFP
Fluorescent
labeling
Blood collection by
cardiac puncture
Adoptive
transfer
Intravital
lung imaging
b)
0.000sec
0.033sec
0.066sec
Time sequence
Tracking
Tie2 DiD-RBC
c)
1500
0
Mean velocity (um/s)
d)
PBS
LPS
Mean velocity of RBC (μm/s)
1,000
800
600
400
200
0
f)
Total capillary area
/ field of view (%)
80
60
40
20
0
g)
Functional capillary area /
Total capillary area (%)
60
40
20
0
*
e)
Capillary
Functional
Merge
PBS
LPS
Tie2
DiD-RBC
Tie2 DiD-RBC
h)
Partial pressure of
arterial O_2 (mmHg)
100
80
60
40
20
0
*
i)
Partial pressure of
arterial CO_2 (mmHg)
80
60
40
20
0
*

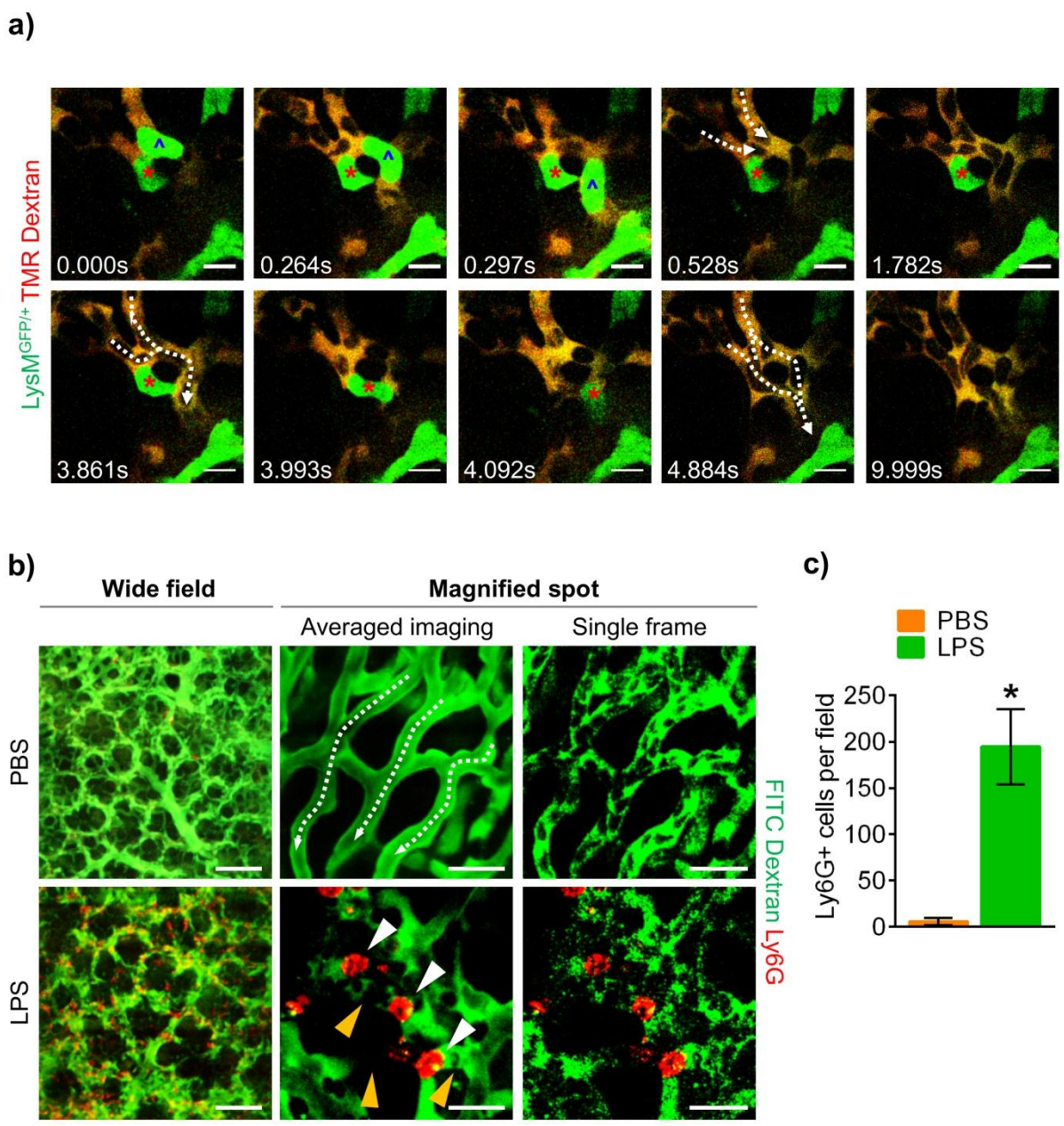
a)
LysM^GFP/+ TMR Dextran
0.000s
0.264s
0.297s
0.528s
1.782s
3.861s
3.993s
4.092s
4.884s
9.999s
b)
Wide field
Magnified spot
Averaged imaging
Single frame
PBS
LPS
FITC Dextran Ly6G
c)
PBS
LPS
Ly6G+ cells per field
250
200
150
100
50
0
*

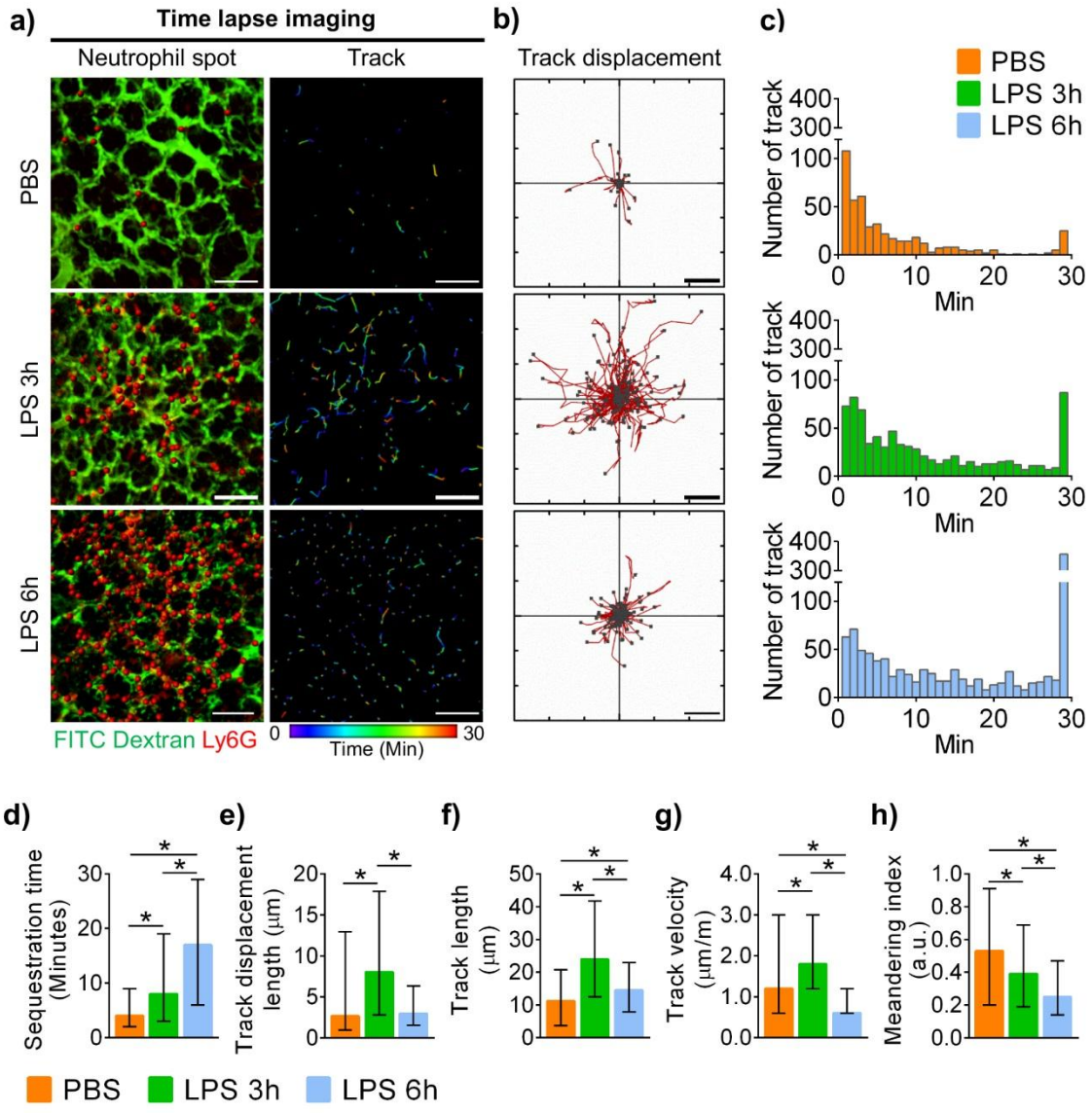
a)
Time lapse imaging
Neutrophil spot
Track
PBS
LPS 3h
LPS 6h
FITC Dextran Ly6G
0
30
Time (Min)
b)
Track displacement
c)
PBS
LPS 3h
LPS 6h
Number of track
Min
d)
Sequestration time (Minutes)
e)
Track displacement length (μm)
f)
Track length (μm)
g)
Track velocity (μm/m)
h)
Meandering index (a.u.)
PBS
LPS 3h
LPS 6h

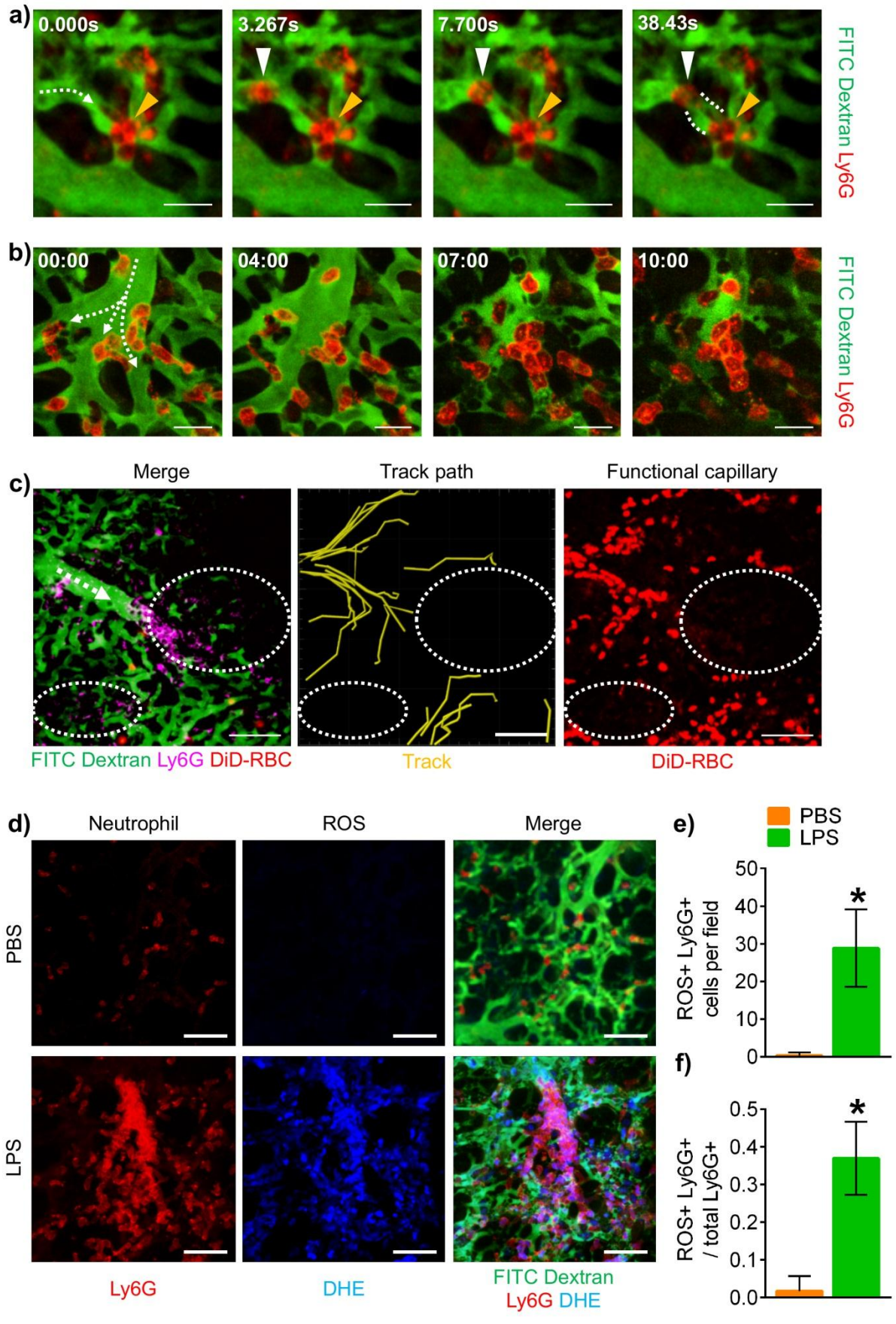
a)
0.000s
3.267s
7.700s
38.43s
FITC Dextran Ly6G
b)
00:00
04:00
07:00
10:00
FITC Dextran Ly6G
c)
Merge
Track path
Functional capillary
FITC Dextran Ly6G DiD-RBC
Track
DiD-RBC
d)
Neutrophil
ROS
Merge
PBS
LPS
Ly6G
DHE
FITC Dextran
Ly6G DHE
e)
PBS
LPS
ROS+ Ly6G+
cells per field
50
40
30
20
10
0
*
f)
ROS+ Ly6G+
/ total Ly6G+
0.5
0.4
0.3
0.2
0.1
0.0
*

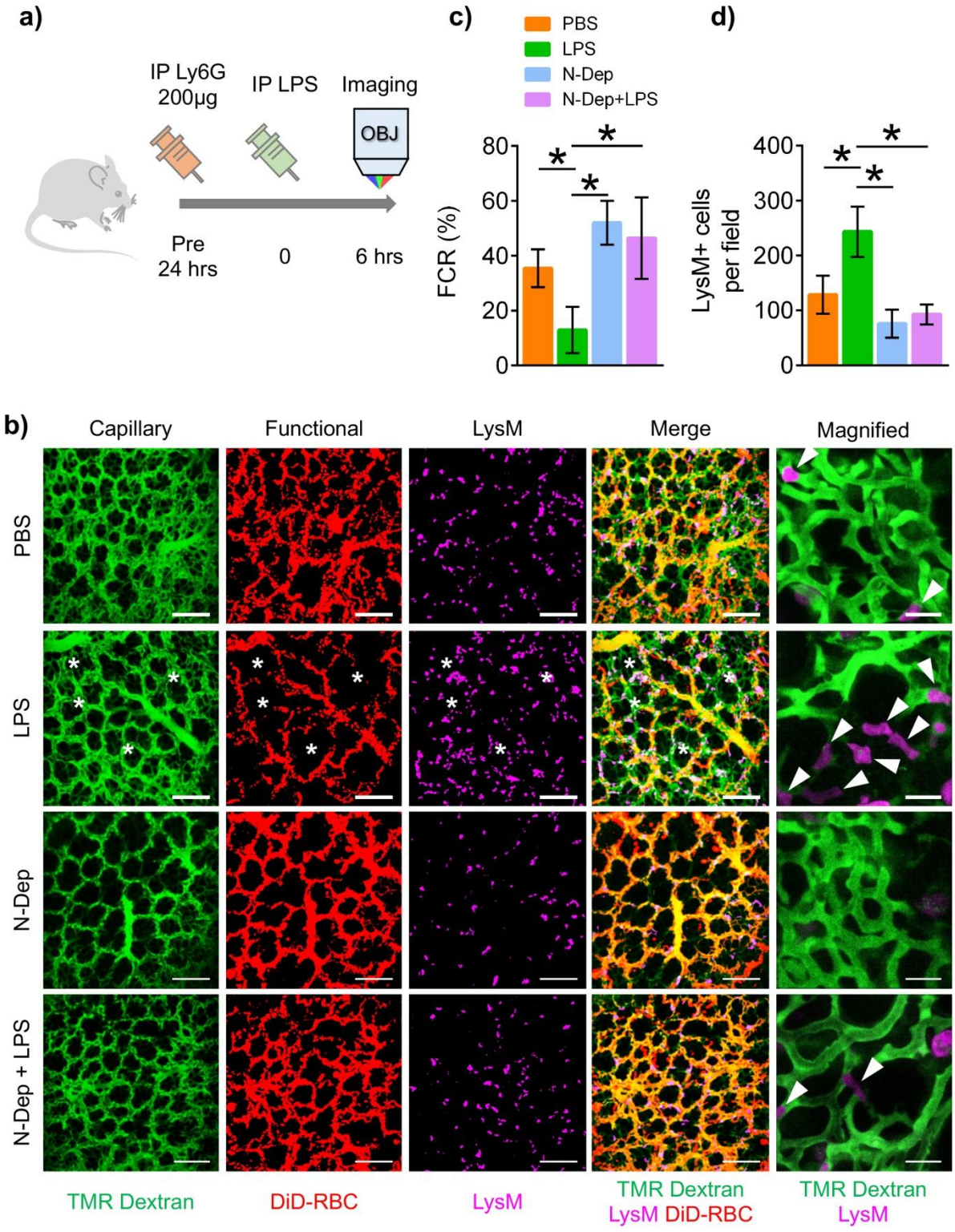
a)
IP Ly6G
200µg
IP LPS
Imaging
OBJ
Pre
24 hrs
0
6 hrs
c)
PBS
LPS
N-Dep
N-Dep+LPS
FCR (%)
80
60
40
20
0
d)
LysM+ cells
per field
400
300
200
100
0
b)
Capillary
Functional
LysM
Merge
Magnified
PBS
LPS
N-Dep
N-Dep + LPS
TMR Dextran
DiD-RBC
LysM
TMR Dextran
LysM DiD-RBC
TMR Dextran
LysM

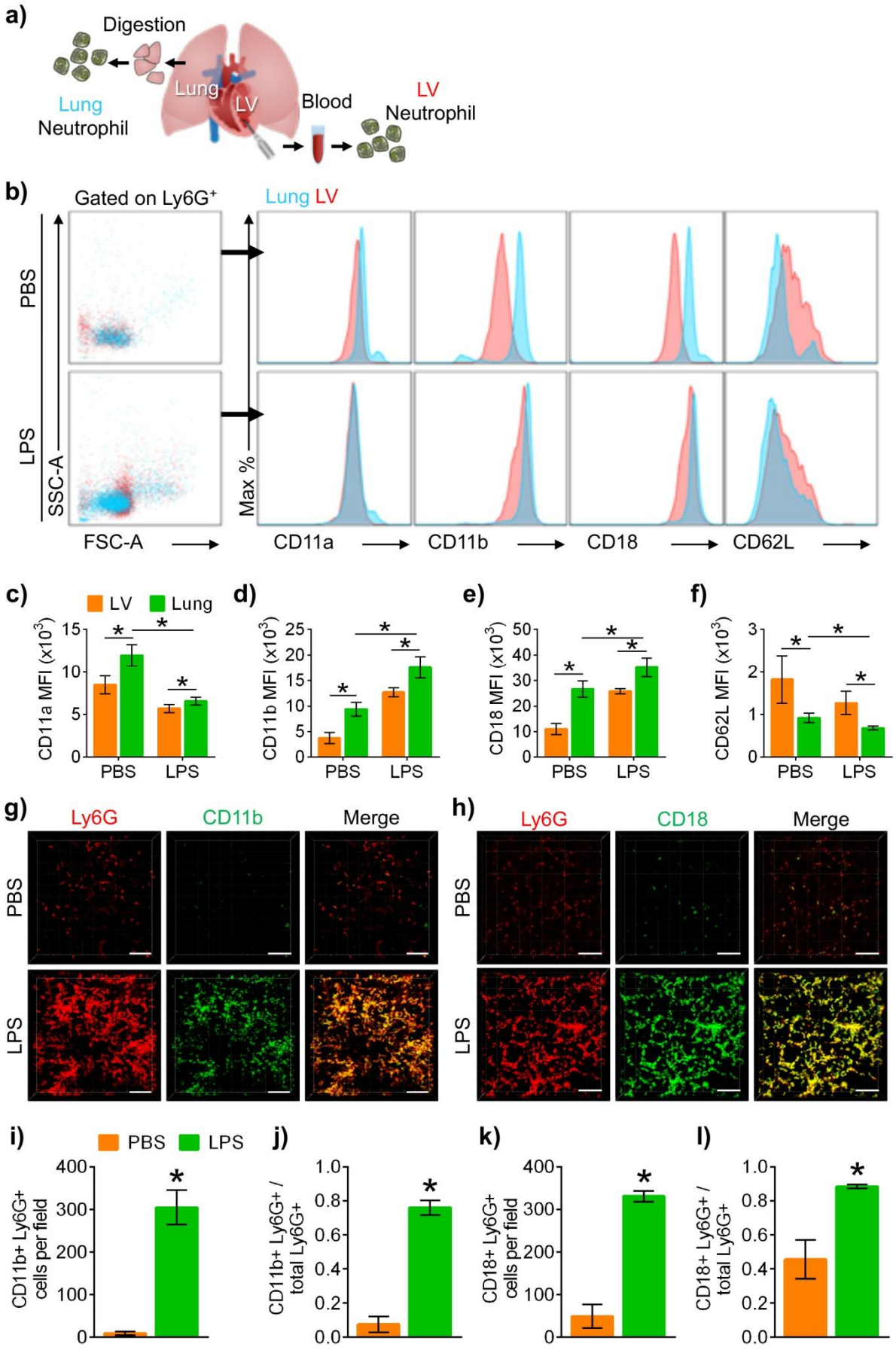
a)
Digestion
Lung
Neutrophil
Lung
LV
Blood
LV
Neutrophil
b)
Gated on Ly6G+
Lung LV
PBS
LPS
SSC-A
FSC-A
Max %
CD11a
CD11b
CD18
CD62L
c)
LV
Lung
CD11a MFI (x10^3)
PBS
LPS
d)
CD11b MFI (x10^3)
e)
CD18 MFI (x10^3)
f)
CD62L MFI (x10^3)
g)
Ly6G
CD11b
Merge
h)
Ly6G
CD18
Merge
i)
PBS
LPS
CD11b+ Ly6G+ cells per field
j)
CD11b+ Ly6G+ / total Ly6G+
k)
CD18+ Ly6G+ cells per field
l)
CD18+ Ly6G+ / total Ly6G+

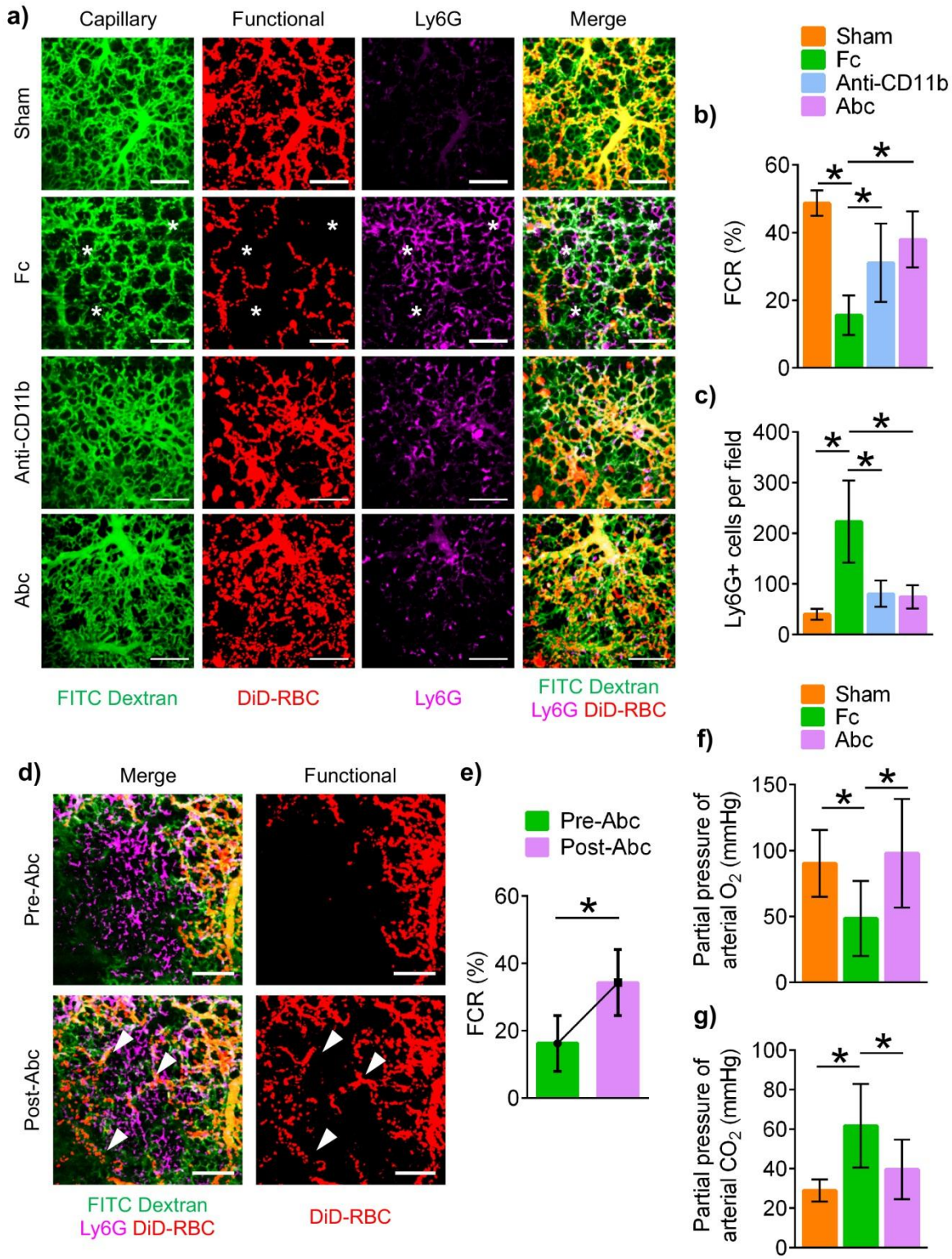
a)
Capillary
Functional
Ly6G
Merge
Sham
Fc
Anti-CD11b
Abc
FITC Dextran
DiD-RBC
Ly6G
FITC Dextran
Ly6G DiD-RBC
b)
Sham
Fc
Anti-CD11b
Abc
FCR (%)
60
40
20
0
c)
Ly6G+ cells per field
400
300
200
100
0
d)
Merge
Functional
Pre-Abc
Post-Abc
FITC Dextran
Ly6G DiD-RBC
DiD-RBC
e)
Pre-Abc
Post-Abc
FCR (%)
60
40
20
0
f)
Sham
Fc
Abc
Partial pressure of arterial O_2 (mmHg)
150
100
50
0
g)
Partial pressure of arterial CO_2 (mmHg)
100
80
60
40
20
0

Supplemental Materials for

Supplemental Materials

Supplemental Video 9. Depletion of neutrophil increases FCR of pulmonary microcirculation.

Supplemental Video 10. Abciximab improves pulmonary microcirculation in sepsis-induced ALI model.

Materials & Methods

Animal Model

To generate sepsis-induced ARDS model, high-dose LPS or CLP model was utilized. For high-dose LPS model, LPS (10mg/kg, *E. coli* serotype 055:B5, L2880, Sigma-Aldrich) was intraperitoneally administered to peritoneum before 3 to 6 hours of imaging. In the control group, the same amount of PBS was injected into the peritoneum. High-grade CLP was performed by a single experienced operator according to the previously described method [45]. 75% of the cecum was ligated with 6-0 black silk, and single puncture with a dual hole in distal cecum was made with a 21-gauge needle. After puncture, the cecum was gently squeezed to confirm the patency of puncture hole for extrusion of feces. The cecum was replaced to the abdominal cavity, and abdominal incision was closed with 4-0 black silk. The sham group underwent the same surgical procedure except for the cecal ligation and puncture.

Fluorescent dye and antibody utilized in intravital imaging

Erythrocyte was acquired by cardiac puncture and then labeled with Vybrant DiD (V22887, ThermoFisher Scientific) following the method described in product information sheet. 50 million counts of DiD-labeled erythrocyte was injected via a vascular catheter in tail vein right before imaging [46]. To visualize the vessel with a fluorescent dye, FITC (Molecular Weight 2M Da, Sigma-Aldrich) or Tetramethylrhodamine (TMR) conjugated dextran dye (Molecular Weight 40 KDa, ThermoFisher Scientific) was injected via same vascular catheter described above. To specifically label the neutrophil *in vivo*, 25 μg of Anti-Ly6G+ monoclonal antibody (Clone 1A8, 551459, BD) conjugated with a fluorophore Alexa Fluor 555 or 647 (A-20005 / A-20006, ThermoFisher Scientific) was injected via tail vein 2 hours before imaging. To visualize the molecular expression of pulmonary sequestered neutrophil

in vivo, 25 μg of CD11b (Clone M1/70, 553307, BD Biosciences) and CD18 (Clone GAME-46, 555280, BD Biosciences) conjugated with Alexa 555 was injected via tail vein 2 hours before imaging. DHE was prepared in a manner written in previous intravital studies except for higher dosages (10 mg/kg) [47]. For neutrophil depletion model, 200 μg of Anti-Ly6G monoclonal antibody (Clone 1A8, 551459, BD Biosciences) was injected intraperitoneally 24 hours before sepsis-induced ARDS modeling [48]. For Mac-1 inhibitor model, Anti-CD11b [49] (5 mg/kg, Clone M1/70, 553307, BD Biosciences) and Abciximab [50, 51] (10 mg/kg, Clotinab, ISU Abxis) were injected intraperitoneally 1 hour after CLP modeling which was 5 hours before intravital imaging. To compare the pre-abciximab and post-abciximab FCR, intravital imaging was performed 6 hours after CLP, and FCR imaging of pre-abciximab setting was acquired, and then abciximab was injected. At 30 minutes after the abciximab injection, FCR imaging of post-abciximab was performed.

Flow Cytometry

For flow cytometry analysis, neutrophil was isolated from blood collected from left ventricle and lung. To isolate pulmonary sequestered neutrophils, lungs were harvested and digested without perfusion. Lungs were placed in PBS solution, minced and filtered through a 40μm filter and stained with antibody for 30 minutes at 4°C. Antibody clones used in this studies: Ly6G-FITC (1A8, 551460, BD Biosciences), CD11a-BV510 (M17/4, 563669, BD Biosciences) CD11b-PE-Cy7 (M1/70, 552850, BD Biosciences), CD18-APC (C71/16, 562828, BD Biosciences), CD62L (MEL-14, 560514, BD Biosciences), Viability Dye eFluor 506 (65-0866-14, ThermoFisher Scientific). Stained cells were analyzed with LSR Fortessa flow cytometer (BD Biosciences). Analysis for flow cytometry was performed with Flowjo (FlowJo, LLC)

Histological Analysis

To validate neutrophil depletion in the lung of $LysM^{GFP/+}$ mouse, lungs were harvested after intravital imaging. Perfusion and fixation with 4% paraformaldehyde were performed and further fixed overnight in 4% paraformaldehyde. For hematoxylin and eosin (H&E) staining, tissues were processed using standard procedures, embedded in paraffin, and sliced into 4μm sections followed by conventional H&E staining.

Arterial Blood Gas Analysis

To assess the partial pressure of O_2 and CO_2 in arterial blood to evaluate the oxygenation status, arterial blood gas analysis was performed. 1ml syringe with 22 gauge needle was coated with heparin and introduced into a left ventricle of the heart. Approximately 200 μl of blood was sampled and analyzed with i-STAT handheld blood analyzer (G3 cartridge, Abbott Point of Care Inc). Animals were euthanized with CO_2 chamber right after blood sampling.

Wet-to-dry weight Ratio

To assess the pulmonary edema in mice, the wet-to-dry weight ratio was performed. At 6 hours and 24 hours of injury with the Mac-1 inhibitor experimental model described as above, the entire unlavaged lung was harvested and immediately weighed (wet weight) and reweighed after keeping in a 60 °C drying oven for 72 hours (dry weight).

Imaging System

To visualize *in vivo* pulmonary microcirculation through the window, a custom-built video-rate laser-scanning confocal microscopy system was implemented [52-56]. Three continuous laser modules (Wavelength at 488 nm (MLD488, Cobolt), 561 nm (Jive, Cobolt), and 640 nm (MLD640, Cobolt)) were utilized as excitation light source for multi-color fluorescence

imaging. Laser beams were collinearly integrated by dichroic beam splitters (DBS1; FF593-Di03, DBS2; FF520-Di02, Semrock) and transferred to the laser-beam scanner by a multi-edge dichroic beam splitter (DBS3; Di01-R405/488/561/635, Semrock). The laser scanning section consisted of 2 axises - X-axis scanning with a rotating polygonal mirror with 36 facets (MC-5, aluminum coated, Lincoln Laser) and Y-axis scanning with a galvanometer scanning mirror (6230H, Cambridge Technology). The two-dimensional raster scanning laser beam was transferred to the lung of mice through the commercial objective lens (LUCPLFLN, 20X, NA 0.45, Olympus, LUCPLFLN, 40X, NA 0.6, Olympus, LCPLFLN100XLCD, 100X, NA 0.85, Olympus). The fluorescence signal emitted from the lung of the mice on XYZ translational 3D stage (3DMS, Sutter Instrument) were epi-detected by the objective lens. De-scanned three-color fluorescence signals were spectrally divided by a dichroic beam splitter (DBS4; FF560-Di01, DBS5; FF649-Di01, Semrock) and then detected by photomultiplier tubes (PMT; R9110, Hamamatsu) through bandpass filters (BPF1; FF02-525/50, BPF2; FF01-600/37, BPF3; FF01-685/40, Semrock). The voltage outputs of each PMTs were digitalized by a 3-channel frame grabber (Solios, Matrox) with 8-bit resolution at the sampling rate of 10 MHz. Using a custom-written imaging software based on Matrox Imaging Library (MIL9, Matrox) and Visual C#, video-rate movies were displayed and recorded in real time at the frame rate of 30Hz and frame size of 512 x 512 pixels.

Intravital Pulmonary Imaging

The detailed description is provided in the previous study [57]. All the mice were anesthetized with Ketamine (80 mg/kg) and Xylazine (12 mg/kg). After anesthesia, using a lightning guidewire, intubation with 20 Gauge vascular catheter was performed and connected to a mechanical ventilator (MouseVent, Kent Scientific). Ventilation was

conducted in the setting of the inspiratory pressure of 24~30 mmHg, a respiratory rate of 120~130 breaths per minute, and a positive-end expiratory pressure of 2 cmH_2O. Isoflurane was delivered with 2% to maintain anesthesia status, and pulse oximetry was applied to monitor oxygenation and survival status. Thermal probe of the homeothermic system (RightTemp, Kent Scientific) was introduced into the rectum, and a feedback-regulated heating pad was used to maintain body temperature at 37.0 °C. Tail vein was cannulated with a 30-gauge needle attached to the PE-10 tube for intravenous injection of molecular dye and cell. Then mice were positioned in right lateral decubitus which was followed by dissection of left thoracotomy. Skin and muscle were dissected until rib exposure and incision was made between 3rd and 4th rib to exposure pleura. After thoracotomy, previously mentioned imaging window [58, 59] was applied to the surface of the pleura, and negative suction pressure (20~30 mmHg) provided by a pump (DOA-P704-AA, GAST) and regulator (NVC 2300a, EYELA) was applied via a tube connected to lung imaging window.

Image Processing

Images were displayed and stored at an acquisition rate of 30 frames per second with 512 x 512 pixels per frame. The real-time image frames were averaged over 30 frames by using a MATLAB (Mathworks) code to improve contrast and signal-to-noise ratio. To minimize the motion artifact, each frames were processed with image registration algorithm prior to averaging. Functional capillary imaging analysis was performed using real-time movie of DiD-labeled erythrocytes flowing in capillaries. After splitting colors of movie, sequential images of channels detecting DiD was processed by a median filter with a radius of two pixels to enhance the signal-to-noise ratio. Maximal intensity projection of 600 to 900 (20 – 30 seconds) frames was generated to show the functional capillary perfused by erythrocytes. Functional capillary ratio (FCR) was determined by calculating the ratio of functional

capillary area (DiD-labeled RBC) to the total capillary area (vessel area detected by Tie2 or Dextran signaling). All image processing to calculate FCR was performed by ImageJ (https://imagej.nih.gov/ij/). Image rendering with three-dimensional reconstruction, track analysis of erythrocytes and neutrophils, and plotting track displacement was conducted with IMARIS 8.2 (Bitplane).

Statistical Analysis

All data are presented as mean ± standard deviation (S.D.) or median ± interquartile range, as appropriate to represent values of the group respectively. Statistical differences between means or medians were determined by unpaired 2-tailed Student's t-test, Mann-Whitney test, one-way ANOVA with post hoc Holm-Sidak's multiple comparisons, or Kruskal-Wallis test with post hoc Dunn's multiple comparison tests, as appropriate. Statistical significance was set at $P < 0.05$, and analysis was performed with Prism 6.0 (GraphPad).

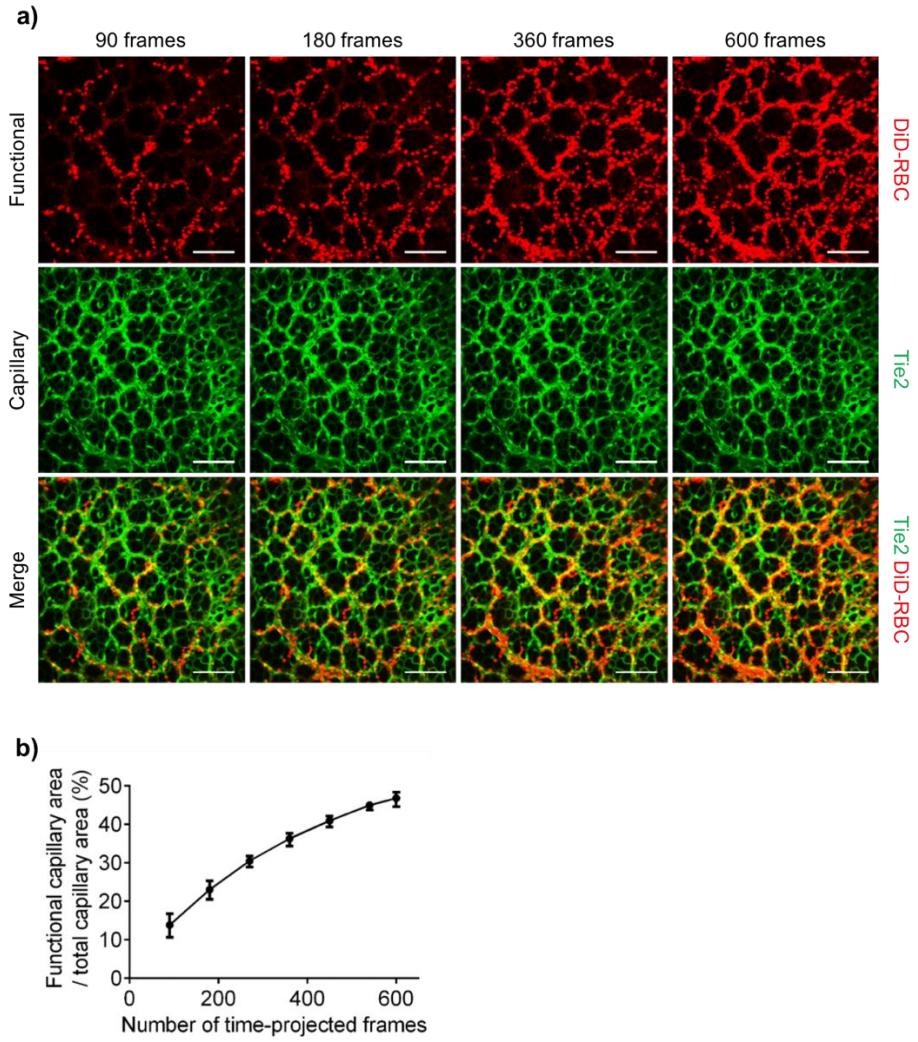

Supplemental Figure 1. Mapping of functional capillary ratio (FCR) according to number of frames.

(**a**) Representative image of functional capillary area revealed by perfusion of DiD-labeled erythrocyte, anatomical capillary revealed by Tie2+GFP+ endothelial cell, and merged image according to the number of maximally projected sequential frames. FCR was generated by calculating the area of anatomical capillary overlapped with the functional capillary area produced with maximal intensity projection of real-time sequential image of DiD-labeled erythrocyte. Scale bars, 100 μm. (**b**) Quantification of FCR in each time-projected frames (*n* = 5 per each group).

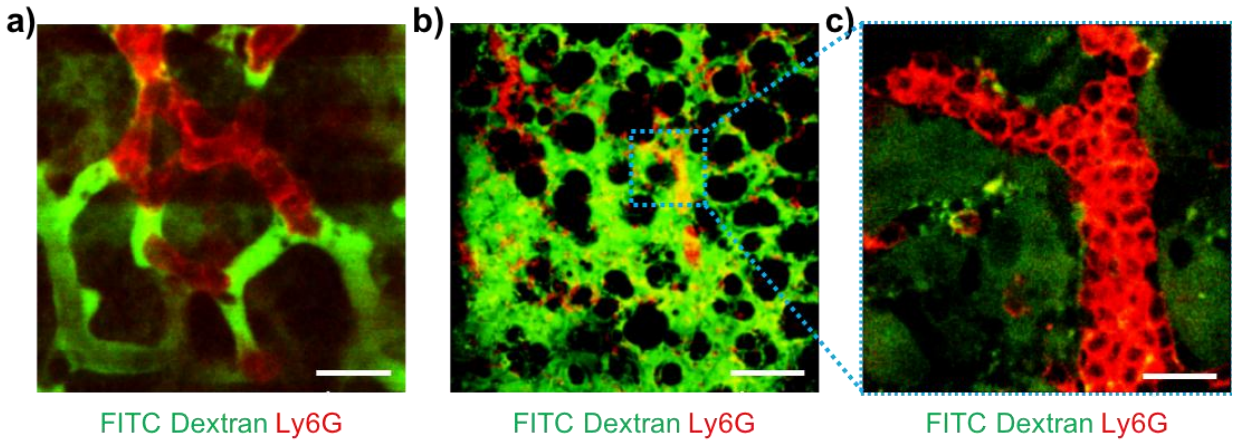

Supplemental Figure 2. Identification of neutrophil aggregates in capillary and arteriole.

(**a**) Representative intravital lung imaging of thrombus formation inside capillary. Scale bar, 20 μm. (**b**) Representative intravital lung imaging of thrombus formation in arteriole and (**c**) magnified image in **b**. Scale bars, 100 μm in **b**, and 20 μm in **c**.

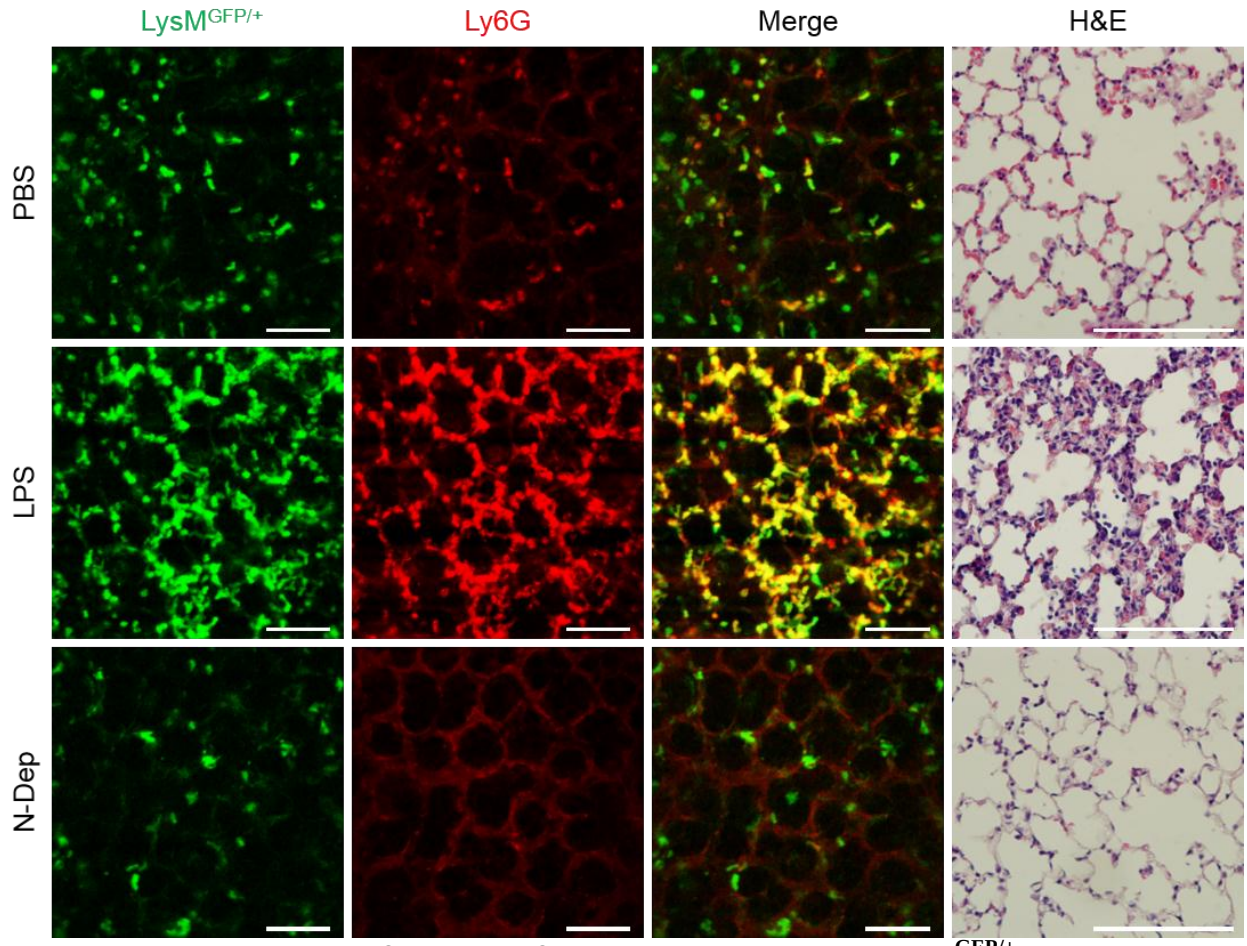

Supplemental Figure 3. Confirmation of neutrophil depletion in LysM$^{GFP/+}$ model.

Representative intravital imaging of neutrophil depletion in PBS and LPS and neutrophil depletion (N-Dep) group. Intravital imaging was performed 6 hours after intraperitoneal PBS or LPS injection. Intravital imaging of N-dep model was performed 24 hours after intraperitoneal high-dose of anti-Ly6G antibody injection. Neutrophil depletion was confirmed by intravital imaging and histological study of H&E section. Remnant LysM+ cell in N-dep model represents macrophage. Scale bars, 100 μm

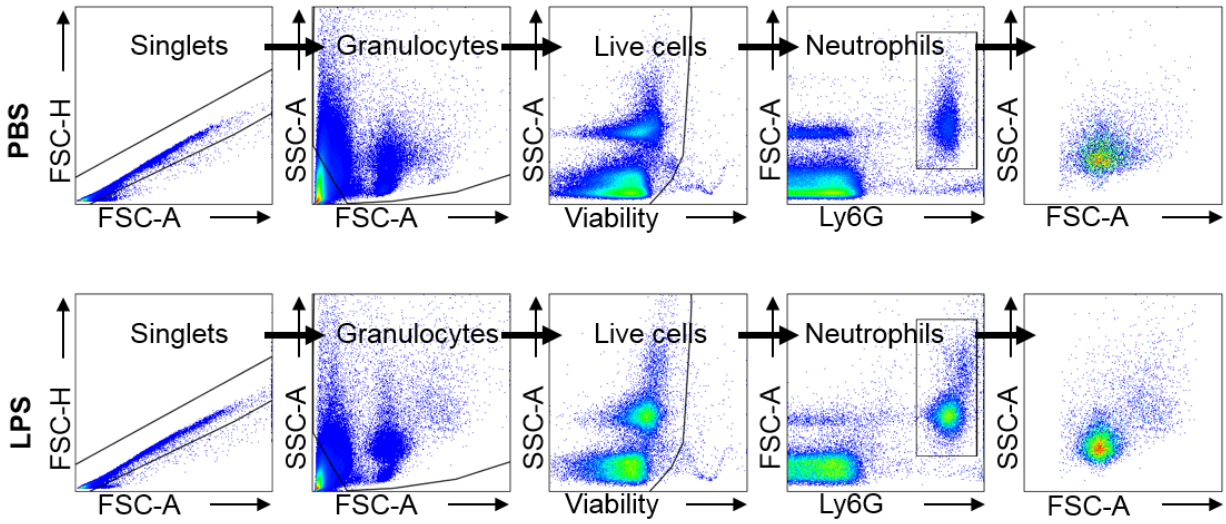

Supplemental Figure 4. Flow cytometry gating strategy to isolate neutrophil.

Representative flow cytometry gating strategy to identify surface expression of neutrophil in PBS and LPS group.

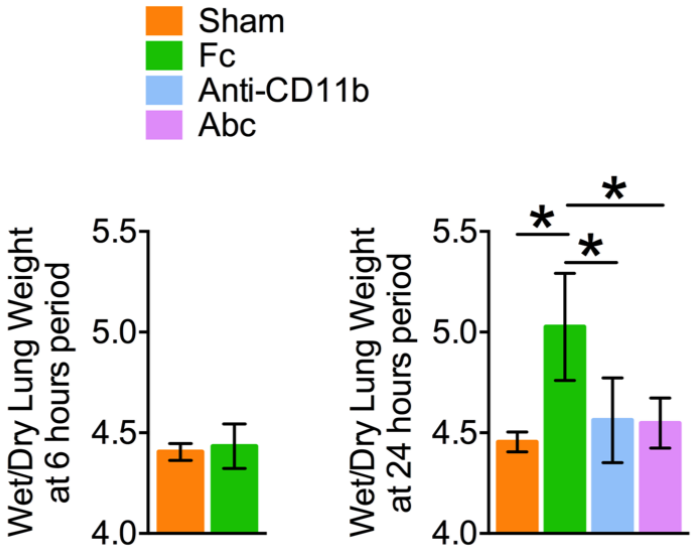

Supplemental Figure 5. Assessment of pulmonary edema in Mac-1 inhibition.

Comparisons of wet-to-dry weight ratios of the lung in sham, CLP, CLP with Anti-CD11b, and CLP with Abciximab treatment group at 6 and 24 hours after lung injury. Significant amelioration of lung edema by Mac-1 inhibition was identified at 24 hours after injury while no difference was identified at the early stage of injury (6 hours) [60, 61]. (n = 4 and 6 mice in 6 hours ; 5, 8, 4, and 7 mice in 24 hours, * $P < 0.05$, Mann-Whitney test). Data are means ± s.d..

Supplementary References

45. Rittirsch D, Huber-Lang MS, Flierl MA, Ward PA. Immunodesign of experimental sepsis by cecal ligation and puncture. *Nat Protoc* 2009: 4(1): 31-36.

46. Seo H, Hwang Y, Choe K, Kim P. In vivo quantitation of injected circulating tumor cells from great saphenous vein based on video-rate confocal microscopy. *Biomed Opt Express* 2015: 6(6): 2158-2167.

47. Finsterbusch M, Hall P, Li A, Devi S, Westhorpe CL, Kitching AR, Hickey MJ. Patrolling monocytes promote intravascular neutrophil activation and glomerular injury in the acutely inflamed glomerulus. *Proc Natl Acad Sci U S A* 2016: 113(35): E5172-5181.

48. Daley JM, Thomay AA, Connolly MD, Reichner JS, Albina JE. Use of Ly6G-specific monoclonal antibody to deplete neutrophils in mice. *J Leukoc Biol* 2008: 83(1): 64-70.

49. Ahn GO, Tseng D, Liao CH, Dorie MJ, Czechowicz A, Brown JM. Inhibition of Mac-1 (CD11b/CD18) enhances tumor response to radiation by reducing myeloid cell recruitment. *Proc Natl Acad Sci U S A* 2010: 107(18): 8363-8368.

50. Peter K, Schwarz M, Conradt C, Nordt T, Moser M, Kubler W, Bode C. Heparin inhibits ligand binding to the leukocyte integrin Mac-1 (CD11b/CD18). *Circulation* 1999: 100(14): 1533-1539.

51. Schwarz M, Nordt T, Bode C, Peter K. The GP IIb/IIIa inhibitor abciximab (c7E3) inhibits the binding of various ligands to the leukocyte integrin Mac-1 (CD11b/CD18, alphaMbeta2). *Thromb Res* 2002: 107(3-4): 121-128.

52. Rajadhyaksha M, Anderson RR, Webb RH. Video-rate confocal scanning laser microscope for imaging human tissues in vivo. *Appl Opt* 1999: 38(10): 2105-2115.

53. Veilleux I, Spencer JA, Biss DP, Cote D, Lin CP. In Vivo Cell Tracking With Video Rate Multimodality Laser Scanning Microscopy. *IEEE Journal of Selected Topics in Quantum Electronics* 2008: 14(1): 10-18.

54. Choe K, Jang JY, Park I, Kim Y, Ahn S, Park DY, Hong YK, Alitalo K, Koh GY, Kim P. Intravital imaging of intestinal lacteals unveils lipid drainage through contractility. *J Clin Invest* 2015: 125(11): 4042-4052.

55. Choe K, Hwang Y, Seo H, Kim P. In vivo high spatiotemporal resolution visualization of circulating T lymphocytes in high endothelial venules of lymph nodes. *J Biomed Opt* 2013: 18(3): 036005.

56. Ahn J, Choe K, Wang T, Hwang Y, Song E, Kim KH, Kim P. In vivo longitudinal cellular imaging of small intestine by side-view endomicroscopy. *Biomed Opt Express* 2015: 6(10): 3963-3972.

57. Park I, Choe K, Seo H, Hwang Y, Song E, Ahn J, Hwan Jo Y, Kim P. Intravital imaging of a pulmonary endothelial surface layer in a murine sepsis model. *Biomed Opt Express* 2018: 9(5): 2383-2393.

58. Looney MR, Thornton EE, Sen D, Lamm WJ, Glenny RW, Krummel MF. Stabilized imaging of immune surveillance in the mouse lung. *Nat Methods* 2011: 8(1): 91-96.

59. Lamm WJ, Bernard SL, Wagner WW, Jr., Glenny RW. Intravital microscopic observations of 15-microm microspheres lodging in the pulmonary microcirculation. *J Appl*

Physiol (1985) 2005: 98(6): 2242-2248.

60. Carraway MS, Piantadosi CA, Jenkinson CP, Huang YC. Differential expression of arginase and iNOS in the lung in sepsis. *Exp Lung Res* 1998: 24(3): 253-268.

61. Wang Q, Wu X, Tong X, Zhang Z, Xu B, Zhou W. Xuebijing Ameliorates Sepsis-Induced Lung Injury by Downregulating HMGB1 and RAGE Expressions in Mice. *Evid Based Complement Alternat Med* 2015: 2015: 860259.